# On the Two-Phase Structure of Protogalactic Clouds[1]

D. N. C. Lin[2] & S. D. Murray[3]

[1]Lick Observatory Bulletin No.

## ABSTRACT

In the gaseous envelope of protogalaxies, thermal instability leads to the formation of a population of cool fragments which are confined by the pressure of a residual hot background medium. In order to remain in a quasi-hydrostatic equilibrium, the residual gas evolves at approximately the virial temperature of the dark matter halo. Its density is determined by the requirements of thermal equilibrium. The hot gas is heated by compression and shock dissipation. The heating is balanced by direct energy loss due to bremsstrahlung emission, and by conductive losses into the cool clouds, which are efficient radiators. The cool fragments are photoionized and heated by the extragalactic UV background and nearby massive stars. Several processes interact to determine the size distribution of the cool fragments. The smallest are evaporated due to conductive heat transfer from the hot gas. All fragments are subject to disruption due to hydrodynamic instabilities. The fragments also gain mass due to collisions and mergers, and condensation from the hot gas due to conduction. The size distribution of the fragments in term determines the rate and efficiency of star formation during the early phase of galactic evolution. We have performed one-dimensional hydrodynamic simulations of the evolution of the hot and cool gas. The cool clouds are assumed to follow a power-law size distribution, and fall into the galactic potential, subject to drag from the hot gas. The relative amounts of the hot and cool gas is determined by the processes discussed above, and star formation occurs at a rate sufficient to maintain the cool clouds at $10^4$ K. We present density distributions for the two phases and also

[2]UCO/Lick Observatory, University of California, Santa Cruz, CA, 95064
Electronic mail: lin@ucolick.org

[3]Lawrence Livermore National Laboratory, L-22, P.O. Box 808, Livermore, CA, 94550
Electronic mail: sdmurray@llnl.gov

for the stars for several cases, parametrized by the circular speeds of the potentials. Under some conditions, primarily low densities of the hot gas, conduction is more efficient than radiative processes at cooling the hot gas, limiting the x-ray radiation from the halo gas.

## 1. Introduction

According to CDM models of galaxy formation (Blumenthal et al. 1984; Navarro, Frenk, & White 1997; Klypin, Nolthenius, & Primack 1997), large galaxies emerge through the coalescence of smaller systems, normally identified as dwarf galaxies, which contain mostly dark matter with a fraction of gas. The dark matter components merge with each other in a dissipationless manner to form the halos of larger galaxies. The crossing of gas streamlines leads to shocks, heating the gas to the virial temperature of the galactic halo (Binney 1977; Rees & Ostriker 1977; White & Rees 1978). In order for the heated gas in this extended halo (hereafter, the protogalactic cloud or PGC) to collapse, its cooling timescale $\tau_c$ must be shorter than its dynamical time scale, $\tau_d$ during each growth stage of the galaxy. When large galaxies acquire a mass comparable to the Galaxy, this condition is satisfied once the characteristic length scale of the PGC is $< 100$ kpc (Blumenthal et al. 1984).

For typical values ($\sim 10^6$ K) of the virial temperature, the cooling timescale increases with temperature, and the PGC's are thermally unstable (Field 1965). Thermal instability leads to the rapid growth of perturbations and fragmentation of PGCs (Murray & Lin 1990). The result is that a two-phase medium develops during the initial cooling of the PGC, in which a population of warm fragmentary clouds (WFC's) are confined by the pressure of hot, residual halo gas (RHG) (Burkert & Lin 2000). The RHG is primarily heated by the release of the gravitational energy of the collapsing PGC and cooled by radiative emission and conductive transport. The WFC's settle into the central region of the halo potential. They are unable to cool below $10^4$ K until their density reaches a sufficiently high value that the WFC's become self-shielded from external photodissociating UV radiation (Couchman & Rees 1986; Haiman, Rees, & Loeb 1997; Haiman, Abel, & Rees in press). Thereafter, molecular hydrogen can form within them as a consequence of non-equilibrium cooling. Efficient cooling reduces the temperature to $T < 100$ K even in the absence of metals. Consequently, WFC's evolve into cold molecular clouds (CMCs). The formation of massive stars within the CMC's provides ultraviolet heating, limiting the formation rate of CMC's from WFC's, and leading to the formation of an equilibrium three-phase structure in the galaxy. In this paper, we discuss the evolution of the hot phase that is left after the initial thermal instability. Detailed investigations of the warm and cold phases will be made in upcoming papers. For the current work, we assume a power-law size distribution for the WFC's. The CMC's are not included explicitly, but star formation within them is explicitly assumed to occur at a rate which would provide an adequate flux of UV photons to heat and ionize the WFC's.

In §2, we briefly recapitulate the physical processes associated with this scenario. In § 3,

we determine the energy balance between the warm and hot phases, while in § 4, we discuss the resulting star formation rate in the WFC's. In § 5, we show model results on the evolution of the warm and hot phases. Finally, we summarize our results and discuss their implications in § 6.

## 2. The Emergence of a Two-phase Medium

The temperature of a large, virialized PGC, $T \sim V_c^2 \mu/k \simeq 10^6 (V_c/100 \text{ km sec}^{-1})^2$ K, where $V_c$ is the circular velocity of the halo potential, $\mu$ is the mean atomic weight in grams, and $k$ is the Boltzmann constant. At such temperatures, the dominant radiative cooling mechanisms are bremsstrahlung and recombination processes (Dalgarno & McCray 1972). The radiative cooling rates for metal poor clouds (with [Fe/H]$\lesssim -2$) are

$$\Lambda(T) \approx 10^{-22} \left(\frac{T}{10^5 \text{ K}}\right)^{-1.2} \text{ ergs cm}^3 \text{ s}^{-1} \tag{1}$$

for $2 \times 10^4$ K $< T < 10^6$ K, and

$$\Lambda(T) \approx 6 \times 10^{-24} \left(\frac{T}{10^6 \text{ K}}\right)^{1/2} \text{ ergs cm}^3 \text{ s}^{-1} \tag{2}$$

for $T \gtrsim 10^6$ K. Equation (1) is a highly simplified average representation of the behavior of the cooling rate in the given temperature range. In actuality, there is a peak due to H emission at $2 \times 10^4$ K, another due to emission by $He^+$ at $10^5$ K, and a minimum at $\approx 10^6$ K, before the cooling efficiency rises again, due to bremsstrahlung emission (Gould & Thakur 1970).

The cooling timescale is

$$\tau_c = \frac{\frac{3}{2}\rho k T}{\mu n^2 \Lambda} \tag{3}$$

where $\rho$ and $n$ are the mass and number density of the gas. The necessary collapse condition, $\tau_c \leq \tau_d$ where the dynamical timescale $\tau_d = R/V_c$ (White & Rees 1978), for a virialized PGC is satisfied when $n$ exceeds a critical value

$$n_{crit} \approx 0.2 \; R_{kpc}^{-1} \left(\frac{T}{10^6 \text{ K}}\right)^{\frac{1}{2}} \text{ cm}^{-3}, \tag{4}$$

where $R_{kpc} = R/1$ kpc, and R is the galactocentric radius.

Above $3 \times 10^4$ K, $\tau_c$ is an increasing function of $T$, such that the contrast between slightly cooler regions and the background grows during the cooling process. The relatively rapid loss of entropy also leads to a deficit of pressure, $P$, in the clouds compared to their background. The higher pressure of the background compresses the clouds in an attempt to maintain pressure balance. The rise in $n$ leads to a reduction in $\tau_c$ for the clouds, further enhancing the dichotomy in cooling timescale between the clouds and the background. The interface separating cool clouds from the background retreats at an accelerating pace. Although $\tau_c \sim \tau_d$ at the onset of thermal

runaway, it decreases rapidly to $\ll \tau_d$ as the perturbed region cools significantly below the virial temperature.

Clouds, with radius $S$ and sound speed $c_s$, establish hydrostatic equilibrium with the RHG and undergo isobaric evolution on a timescale $\sim S/c_s$. If this timescale is $> \tau_c$, $n$ cannot adjust such that cooling is isochoric. Relatively large clouds undergo a transition from isobaric to isochoric cooling before their density becomes significantly larger than that of the background. This transition in small clouds occurs at a later cooling stage. Their density growth becomes nonlinear before the cooling becomes isochoric. Consequently, they emerge as dense, cool fragments (Burkert & Lin 2000).

When $T$ in the clouds decreases to $\sim 10^4$K, recombination becomes the dominant cooling process. However, these clouds are also exposed to UV radiation due to emission from background active galactic nuclei. At redshift $z = 2.5$, the flux of this emission at the Lyman limit is estimated to be $F_{UV} = 0.5 \times 10^{-21}$ ergs Hz$^{-1}$ ster $^{-1}$ cm$^{-2}$ s$^{-1}$, with a dropoff towards higher energies as steep as $\nu^{-3}$ (Haardt & Madau 1996). The above value varies approximately as $(1 + z)^3$. In the outer regions of PGC where the pressure of the RHG is low, the internal density of these clouds is also relatively small, such that they may be mostly photoionized, with $T \sim 10^4$K. But, in the inner regions of the PGC where the background pressure is higher, WFC's have larger internal density, such that they become self shielded against the extragalactic UV flux and their temperature cools below 100 K due to emission by $H_2$ and metal ions (Dalgarno & McCray 1972; Hollenbach & McKee 1979). When these clouds become gravitationally unstable, stars rapidly form within them. The UV flux provided by these massive stars is able to heat gas within their Strömgren radii to $10^4$ K, quenching star formation in those regions.

At all galactocentric radii, then, the PGC fragments into a population of WFC's which are maintained at $10^4$ K by the UV flux. In most regions, the ionizing photons are emitted by a population of massive stars whose formation rate is self-regulated. The WFC's are embedded within RHG, whose density is sufficiently low that $\tau_c > \tau_d$, ie. it is thermally stable (Field 1965), and it can remain near the virial temperature of the galaxy. The pressure of the RHG confines all but the largest WFC's, for which self gravity is important. Consequently, the PGC becomes a two-phase medium, with the density contrast between the WFC's and the RHG inversely proportional to their temperature ratio ($\sim 100$).

## 3. Energy Budget of the Two-Phase Medium

### 3.1. Dynamical Interaction Between the Warm and Hot Phases

Following its collapse into the potential of the galactic halo, the RHG is shock-heated to the virial temperature of the potential, and rapidly attains a quasistatic equilibrium. It then adjusts to have density and temperature appropriate for the maintenance of thermal equilibrium constrained

by the processes discussed below. The inverse buoyancy of the pressure-confined WFC's causes them to settle towards the center of the potential provided by the dark matter halo. During their descent, the WFC's experience a drag by the RHG, reaching a terminal speed relative to the RHG given by

$$V_t \approx \left( D_\rho \frac{S}{R} \right)^{1/2} V_c, \tag{5}$$

where $D_\rho \equiv \rho_w / \rho_h$ is the ratio of the density of the WFC's to that of the RHGs. (In all relations below, the subscripts "h" and "w" refer to quantities of the RHG and of the WFC, respectively.) For WFC's with sizes $S > R/D_\rho$, $V_t \sim V_c$. Here, we neglect the effect of the clouds' size evolution on their kinematics.

The value of $V_t$ derived in equation (5) assumes a constant density background. In reality, the pressure gradient of the background causes the density of the RHG to rise towards the center of the galaxy. The radii of the WFC's $S \ll R$, and so the pressure gradient across an individual cloud is negligible. If the RHG is approximately isothermal, and the temperature of the WFC's are determined by atomic cooling to be $\approx 10^4$ K, then $D_\rho$ remains constant during the motion of the clouds. As a result, the primary effect of the density gradient of the RHG upon $V_t$ is in altering the ratio $S/R$. If $\rho_h \propto R^{-a}$, then, under the above assumptions, $\rho_w \propto R^{-a}$, $S \propto R^{a/3}$, and $V_t \propto R^{(a-6)/6}$.

The motion of the WFC's through the RHG also leads to mass loss from the WFC's due to Kelvin-Helmholtz instability (Murray et al. 1993). In the limit $D_\rho \gg 1$, the growth timescale of KH instability is given by

$$\tau_{KH} = \lambda \frac{(\rho_h + \rho_w)}{(\rho_h \rho_w)^{1/2} V_t} \approx \frac{\lambda D_\rho^{1/2}}{V_t}. \tag{6}$$

Short wavelength perturbations rapidly saturate. Perturbations with wavelengths $\lambda \approx S$ provide the dominant contribution to mass loss, which occurs at a rate

$$\dot{M} \simeq \frac{4\pi \rho_w S^2 \lambda}{\tau_{KH}} \approx \frac{4\pi \rho_w S^2 V_t}{D_\rho^{\frac{1}{2}}}. \tag{7}$$

For a WFC with a mass $M = 4\pi \rho_w S^3/3$, the stripping timescale $\tau_s = M/\dot{M} \sim (R/3V_c)(S/R)^{1/2} < \tau_d$, *i.e.* WFC's are disintegrated before they settle to the center of the galactic potential. Thus, both thermal instability associated with the cooling, and Kelvin-Helmholtz instability arising during the infall of the WFC's leads to the formation of WFC's with arbitrarily small sizes.

The break down process increases the collective area filling factor of the WFC's, leading to an increase in their collision frequency. Collisions and the resulting mergers increase the masses of the WFC's. When the rates of coagulation and disruption (including other processes discussed below) balance with each other, an equilibrium size distribution is established (Dong et al. in preparation).

### 3.2. Conductive Heat Transfer Between Warm Fragments and Hot Medium

The existence of WFC's in the RHG also leads to heat transfer from the RHG to the WFC's through conduction (McKee & Cowie 1977). This process is particularly important for small WFC's. The conductive heat flux into a WFC is given by

$$F_c = \kappa \nabla T \text{ ergs cm}^{-2} \text{ s}^{-1}, \tag{8}$$

where $\kappa \approx 6 \times 10^{-7} T^{5/2}$ (Spitzer 1956). To order of magnitude,

$$F_c \sim \kappa \frac{T}{l} \approx \left( \frac{1}{3} \kappa_h T_h n_w^2 \Lambda_w \right)^{\frac{1}{2}}, \tag{9}$$

where $l$ is estimated as the depth into the WFC's over which radiative emission balances conduction into the WFC's, and $\Lambda_w$ is the cooling efficiency within the WFC. In terms of the density contrast,

$$F_c \sim \frac{\mu_h}{\mu_w} D_\rho \left( \frac{1}{3} \kappa_h T_h \Lambda_w \right)^{\frac{1}{2}} n_h, \tag{10}$$

where $\mu_h$ and $\mu_w$ are the mean molecular weights in the RHG and WFC's, respectively, and $n_h = \rho_h / \mu_h$. In small clouds where the density scale height is small, the magnitude of $F_c$ is limited by the saturated flux,

$$F_c \simeq F_{sat} = \rho_h c_h^3, \tag{11}$$

where $c_h$ is the isothermal sound speed in the RHG ($\approx 220$ km s $^{-1}$ for the Galaxy). The presence of magnetic field reduces the mean free path of the electrons and $F_c$ (Rosner & Tucker 1989). In our calculations, we neglect the effect of magnetic field and adopt $F_c = F_{sat}$ based on our model parameters.

Large WFC's, which attain large $V_t$, may also advect thermal energy from the RHG to the WFCs at a rate

$$F_a \approx \frac{1}{2} \rho_h V^3. \tag{12}$$

As discussed above, the sizes of the WFC's are modified by Kelvin-Helmholtz instability and coagulation before they are accelerated to $V_t$. The WFC's may therefore spend most of their time with smaller velocities relative to the RHG (Murray et al. 1993). The advective heating is therefore expected to be weaker than that due to conduction.

### 3.3. The Warm Fragmentary Clouds

Energy equilibrium is established within a cloud when

$$\frac{4}{3} \pi S^3 \Gamma_r + 4 \pi S^2 F_c = \frac{4}{3} \pi S^3 n_w^2 \Lambda_w.$$

The photoionization heating

$$\Gamma_r = (1 - x_w) n_w h \int_{\nu_0}^{\infty} \frac{4\pi J_\nu}{h\nu} a_\nu (\nu - \nu_0) d\nu = (1 - x_w) n_w f_G 4\pi J_{\nu_0} a_{\nu_0} \nu_0, \tag{13}$$

where $x_w$ is the ionization fraction in the WFC's, $h$ is Planck's constant, $J_\nu$ is the mean intensity in ergs ster$^{-1}$ Hz$^{-1}$ s$^{-1}$, $a_\nu$ is the photoionization cross section as a function of frequency, $h\nu_0 = 13.6$ eV, and $f_G$ depends upon the shape of the spectrum ($f_G < 0.1$ for realistic background spectra). This equilibrium determines the temperature of the WFC's. The above assumes a top-hat density distribution within the clouds. This is appropriate for clouds which are at most weakly self-gravitating, given the sharp temperature transition between the WFC's and the RHG resulting from thermal instability.

In a mostly ionized WFC, the heat input due to conduction is larger than that due to photoionization when

$$x_w > x_c = 1 - \frac{3}{S} \frac{F_c}{n_w f_G 4\pi J_{\nu_0} a_{\nu_0} \nu_0}. \tag{14}$$

In this limit, the rate of conductive heat input exceeds that of the radiative loss due to recombination when

$$S < S_{es} = \frac{3\mu_h n_h c_h^3}{\Lambda_w n_w^2} \tag{15}$$

in the limit of saturated conduction and

$$S < S_{eu} = \left( \frac{3\kappa_h T_h}{n_w^2 \Lambda_w} \right)^{1/2} \tag{16}$$

in the limit of unsaturated conduction. The above results also apply to the limit in which the background UV flux is negligibly small, so that the gas in WFC's is mostly neutral. For the intermediate case in which photoionization contributes significantly to the heating, the additional energy input would tend to increase the value of $S_{eu}$ and $S_{es}$.

WFC's with $S < S_{es}$ (or $S_{eu}$) are unstable to conductive heat transport. Their inability to radiate away all the conductive heat input leads to an increase in their temperatures. In order to maintain pressure equilibrium with the RHG, these WFC's expand, decreasing their internal density. The increase in $S$ enhances conductive heat transport into the clouds, whereas their cooling efficiency decreases with the decrease in $n_w$. Unless $\Lambda_w$ increases rapidly with $T_w$, conduction then leads to the total evaporation of these small WFC's. The stability criterion can be obtained by analyzing the dependence of $S_{es}$, $S_{eu}$, and $S$ upon $T_w$. If we approximate $\Lambda_w \propto T_w^s$, then from equations 15 and 16 we find that both $S_{es}$ and $S_{eu}$ vary as $T_w^{(2-s)/2}$. As the pressure-confined WFC's are heated and expand, however, their radii vary as $T_w^{1/3}$. The clouds are therefore unstable if $s < 4/3$. In that case, we can picture a cloud with $S = S_{es}$ initially. As it is heated and expands, the steep dependence of $S_{es}$ upon $T_w$ leads to $S < S_{es}$. Radiative cooling can then no longer offset conduction into the cloud, leading to further temperature increase and expansion. The same stability criterion of $s > 4/3$ holds for clouds where $S_{eu}$ is the appropriate

limiting radius. This stability condition is met over the temperature range dominated by hydrogen emission, 9000 K $\leq T_w \leq$ 20,000 K, such that clouds with $S < S_{es}$ or $S < S_{eu}$ remain stable until their temperatures reach 20,000 K. The minimum possible stable cloud size is therefore set by the value of $S_{es}$ or $S_{eu}$ at 20,000 K, where $\Lambda(T)$ is a maximum.

In the above analysis, the WFC's are assumed to be confined by the ambient pressure of the RHG. If the WFC's are able to cool to $T \lesssim 10^2$ K, then self-gravity contributes to the confinement of even relatively small clouds. In this limit, thermal equilibrium between photoionization heating and radiative losses may still be established, but it is unstable because of the negative specific heat of self-gravitating clouds (Murray & Lin 1992). The result is similar to that for non self-gravitating clouds, except that, for a self-gravitating cloud, the radius varies as $T_w^{-1}$, and stability requires $s > 4$, which is, again, only satisfied over a very narrow range of temperatures.

While the lower limit of cloud radii is set by their ability to radiate away the energy flux due to conduction in equations (15) and (16), the upper limit of cloud radii is set by gravitational instability. Low mass clouds are confined by the pressure of the RHG. At higher masses, self-gravity becomes important. Clouds become unstable above a critical mass, which depends upon the external pressure

$$M_{crit} = \left[ 3.15 \left( \frac{kT_w}{\mu_w} \right)^4 \frac{1}{G^3 P_h} \right]^{\frac{1}{2}}, \tag{17}$$

where $P_h$ is the pressure of the RHG, and $T_w$ is the internal temperature of the clouds (Ebert 1955; Bonner 1956). This condition corresponds to an approximate maximum cloud radius of

$$S_{BE} = 1.2 \left( \frac{k}{G} \right)^{\frac{1}{2}} \left( \frac{3}{4\pi} \right)^{\frac{1}{3}} \left( \frac{T_w}{\mu_w} \right) (n_h T_h)^{-\frac{1}{2}}. \tag{18}$$

We have adopted the Bonner-Ebert criterion for stability, rather than the Jeans criterion, due to the fact that the WFC's are pressure-confined. While there might be an apparent inconsistency, in that we assume the WFC's to have nearly constant density, whereas the Bonner-Ebert criterion assumes a density gradient. Had we used the Jeans criterion, however, our value for $S_{BE}$ would be very close to that used above, and so the choice of stability criterion does not affect our results below.

The above results assume that the WFC's are subject only to heating by photoionization and by conduction from the hot gas. In addition, the drag of the clouds through the RHG, and the growth of Kelvin-Helmholtz instability will both lead to additional mechanical energy input into the WFC's which could, in principle, provide additional support for the clouds. These mechanisms are least important, however, in the largest clouds, which experience the least drag, and whose self-gravity stabilizes the growth of deeply-penetrating, long wavelength perturbations by Kelvin-Helmholtz instability (Murray et al. 1993). Stability of the most massive clouds should therefore still be governed by the Bonner-Ebert criterion. Detailed models of clouds moving through background gas will be used in future work to confirm these conclusions.

### 3.4. Total Rate of Conductive Energy Transport

The physical processes involved in determining the mass spectrum of the WFC's will be examined in a future paper. In the results below, we assume that the fragmentation and coagulation of the WFC's leads to a power-law size distribution of the WFC's, in which the number density of clouds within the PGC, $n_c$, per unit cloud radius $S$ is given by

$$\frac{dn_c}{dS} = AS^{\gamma}. \tag{19}$$

The normalization constant, $A$, is related to the spatially averaged density of the warm phase by

$$\langle \rho_w \rangle = \int \frac{4}{3}\pi S^3 \rho_w \frac{\mathrm{d}n_c}{\mathrm{d}S}\mathrm{d}S = \frac{4}{3}\pi\rho_w A \left(\frac{1}{\gamma+4}\right)\left(S_{max}^{\gamma+4} - S_{min}^{\gamma+4}\right) \tag{20}$$

where $S_{max}$ and $S_{min}$ are the maximum and minimum cloud size, respectively. As discussed above, $S_{min}$ is determined by the smallest size of clouds which can radiate away the energy conducted into them from the RHG, while $S_{max}$ is determined by the Bonner-Ebert mass. The value of $A$ is a function of galactocentric radius, whereas we assume $\gamma$ to be the same everywhere within the PGC.

If the clouds follow a distribution close to that observed within Galactic cloud complexes, for which $\gamma = -2.5$ (Scalo 1985; Zinnecker, McCaughrean, & Wilking 1993 ), then the results above and below are dominated by the massive end of the distribution. Alternatively, if the efficiency of cloud disruption is high relative to the rate of coagulation, then the cloud distribution will be dominated by the low-mass end. The determination of which limit is appropriate shall be made in an upcoming paper. In the current work, we treat the size distribution as an uncertainty, and consider two extreme limits. In the first, we assume $\gamma > -3$, and all terms derived both above and below are dominated by the high mass end of the cloud distribution. In the second, we assume $\gamma < -4.5$, and all terms are dominated by the low mass end of the distribution.

The total rate of conductive energy transport per unit volume from the RHG into the WFC's is given by

$$L_{cond} = \int \frac{dn_c}{dS} F_c 4\pi S^2 dS. \tag{21}$$

Using the results above, this becomes

$$L_{cond} = \frac{4\pi A F_c}{\gamma+3}\left(S_{max}^{\gamma+3} - S_{min}^{\gamma+3}\right) \tag{22}$$

For $\gamma > -3$, the above result becomes

$$L_{cond} = 3\left(\frac{\gamma+4}{\gamma+3}\right)\frac{\langle\rho_w\rangle}{\rho_w} F_c S_{BE}^{-1}, \tag{23}$$

while for $\gamma < -4$ it is

$$L_{cond} = 3\left(\frac{\gamma+4}{\gamma+3}\right)\frac{\langle\rho_w\rangle}{\rho_w} F_c S_{es}^{-1}. \tag{24}$$

The above results assume that $S_{max} \gg S_{min}$, where $S_{max} = S_{BE}$ and $S_{min} = S_{es}$. As can be seen by a comparison of equations (15) and (18), $S_{min}/S_{max} \sim 0.01(\Lambda_w/10^{-24})^{-1} n_h^{-1/2}$, and so this is a reasonable approximation. Also, because $S_{BE} \gg S_{es}$, the greater surface-to-volume ratio of the case $\gamma < -4$ leads to a significantly greater cooling rate due to conduction into the WFC's relative to the case with $\gamma > -3$.

### 3.5. The Residual Halo Gas

Equations (23) and (24) give the conductive energy transfer rate from the RHG to the WFC's. The RHG also experiences radiative losses, mainly through bremsstrahlung emission, which occurs at a rate given by equation (2). Using the conductive flux given in equations (23) and (24), we find that conductive losses into the WFC's exceed bremsstrahlung cooling in the limit that

$$n_h^2 < 3\left(\frac{\gamma+4}{\gamma+3}\right)\left(\frac{S_{max}^{\gamma+3} - S_{min}^{\gamma+3}}{S_{max}^{\gamma+4} - S_{min}^{\gamma+4}}\right)\frac{\mu_h}{m u_w}\frac{T_w}{T_h}\frac{c_h^3}{\Lambda_h}\langle\rho_w\rangle. \tag{25}$$

when conduction is saturated, and

$$n_h^2 < \left(\frac{\gamma+4}{\gamma+3}\right)\left(\frac{S_{max}^{\gamma+3} - S_{min}^{\gamma+3}}{S_{max}^{\gamma+4} - S_{min}^{\gamma+4}}\right)\frac{(3\kappa_h T_h \Lambda_w)^{\frac{1}{2}}}{\Lambda_h}\langle\rho_w\rangle \tag{26}$$

when conduction is unsaturated. In the above relations, we assume pressure balance between the warm and hot phases, ie. $n_h T_h = n_w T_w$.

Heat is supplied to the RHG through its own quasi-static contraction. More importantly, heat is also deposited into the RHG as a result of the frictional drag on collapsing WFC's, by which the WFC's are able to transfer a fraction of their gravitational potential energy into thermal energy of the RHG. (In the absence of any drag, the total energy of individual WFC's is approximately conserved as they fall into the galactic halo potential.) The heating per unit volume of a flux of WFC's moving at their terminal speeds is given by

$$\Gamma = \int \frac{V_c^2}{R}\frac{\mathrm{d}n_c}{\mathrm{d}S}\frac{4}{3}\pi\rho_w S^3 V_t \mathrm{d}S. \tag{27}$$

Using $V_t$ from eq (6), the above result becomes

$$\Gamma = \left(\frac{\gamma+4}{\gamma+\frac{9}{2}}\right)\left(\frac{S_{max}^{\gamma+\frac{9}{2}} - S_{min}^{\gamma+\frac{9}{2}}}{S_{max}^{\gamma+4} - S_{min}^{\gamma+4}}\right)\left(\frac{\mu_w T_h}{\mu_h T_w}\right)\frac{V_c^3}{R^{\frac{3}{2}}}\langle\rho_w\rangle. \tag{28}$$

For $\gamma > -4$, the above result is dominated by the contribution of the largest WFC's, for which $V_t$ may become comparable to $V_c$ at small $R$. Whether or not the clouds are able to attain $V_t$ depends upon the ratio of their acceleration timescales to the timescales upon which they are affected by conduction, collisions, or Kelvin-Helmholtz instability. For a cloud to be accelerated to

a speed $\sim V_c$, it must travel a distance $\sim R/2$ in the halo, whereas, Kelvin-Helmholtz instability leads to significant mass loss by the time a cloud has moved through the RHG over a distance of several times its diameter (Murray et al. 1993). Unless the RHG is also contracting with a velocity $V_H \sim V_c$, the massive WFC's may not be able to attain their terminal velocities (Dong et al. in preparation). Instead of $V_t$ above, we parametrize the terminal differential velocity as $fV_c$, with $f$ being a free parameter. Using this prescription, the heating rate is given by

$$\Gamma = \frac{fV_c^3}{R}\langle\rho_w\rangle. \tag{29}$$

In the limit $\gamma < -4.5$, the heating is dominated by drag from low mass clouds, for which $V_t < V_c$. The above result then becomes

$$\Gamma = \left(\frac{\gamma+4}{\gamma+\frac{9}{2}}\right)\frac{V_c^3}{R^{\frac{3}{2}}}\left(\frac{\mu_w T_h}{\mu_h T_w}\right)^{\frac{1}{2}}\langle\rho_w\rangle S_{es}^{\frac{1}{2}}. \tag{30}$$

If the radiative and conductive cooling of the RHG exceed the thermal energy input, some of the RHG will precipitate to form additional WFC's. As the gas density of the RHG is depleted, both the conductive heat flux into, and drag on the infalling WFC's decrease. The density $n_h$ therefore adjusts so as to achieve thermal equilibrium in which $G \simeq L_{cond} + L_{brem}$.

## 4. Ionization of the clouds

### 4.1. The Nature of the External Source

In the above analysis, the WFC's are generally taken to be highly ionized. To maintain this ionization state, the UV flux to which the WFC's are exposed must be sufficiently large to offset recombination. In Figure 1, we show the depths into which a cloud may be ionized by various sources of UV flux, plotted as a function of $n$. These results were obtained with CLOUDY (Ferland 1991). The solid, dashed, and dot-dashed curves represent results obtained with the standard AGN spectral energy distribution, for three values of $F_{UV}$. The solid curve was calculated using a value of $0.5 \times 10^{-21}$ ergs Hz$^{-1}$ ster$^{-1}$ cm$^{-2}$ s$^{-1}$ at 13.6 eV, representing the UV background at z=2.5 (Haardt & Madau 1996). The dashed and dot-dashed curves were computed using fluxes that were, respectively, smaller and larger by an order of magnitude, approximately representing redshifts $< 0.5$ and 5 respectively. The dotted curve was computed using the Kurucz spectrum in CLOUDY, with the flux set to that of an O5 star at a distance of 10 pc.

From Figure 1, we can infer the integrated depth into the PGC outside of which all of the warm fragments are ionized. In the early evolutionary epochs of the Galaxy before most of the ordinary matter was converted into stars, only the regions outside $\sim 30$ kpc are photoionized by the UV background (see below). At smaller galactocentric radii, local sources of UV radiation are

required. In diffuse and low mass dwarf galaxies, however, the entire galaxy may be photoionized by the diffuse background radiation (Kepner, Babul, & Spergel 1997).

In addition to the extragalactic background, the RHG radiates soft X-ray photons following a bremsstrahlung spectrum. Previous work (Fall & Rees 1985), which used analytic approximations to estimate the structure of the RHG, found the resulting x-ray flux to be insufficient to ionize large clouds beyond a few kpc from the Galactic center. In the models presented below, we find the bremsstrahlung luminosities to be less than estimated by Fall & Rees (1985). Ionization by the RHG is therefore not a significant contributor to determining the state of the WFC's.

Hydrodynamic drag on WFC's also leads to energy input into them, as described in § 3.4. For relatively large WFC's $V_t > 10$ km s$^{-1}$. If these fragments are not ionized initially, then shocks will cause internal heating. From above, though, the ratio of heating by drag to that by conduction is found to be

$$\frac{\frac{\pi}{2}\rho_1 S^2 V_t^3}{4\pi S^2 F_c} = 3 \times 10^{-4} \left(\frac{V_t}{10 \text{ km s}^{-1}}\right)^3. \tag{31}$$

Thus, even for velocities as high as 100 km s$^{-1}$, the heating rate due to drag is negligible. For survivable clouds with $S > S_{eu}$ and $S_{es}$, conduction does not provide adequate heat transfer to offset radiative loses. Since the dominant radiative process at $\sim 10^4$K is recombination, conductive heat flow is also insufficient to ionize the WFC's.

### 4.2. Self-Regulated Star Formation

In the absence of an adequate ionizing photon flux, the cooling efficiency of bremsstrahlung, recombination, and atomic hydrogen emission decrease rapidly below $\sim 10^4$ K. In a metal-free protogalactic cloud, however, non-equilibrium recombination leads to the formation of a small amount of $H^-$ ions which recombine with neutral $H$ to form $H_2$. Radiative losses due to rotational and vibrational transitions of $H_2$ reduce the gas temperature to $\sim 10^2$ K (Murray & Lin 1990). If [Fe/H]$> -3$, even lower temperatures ($\sim 10$ K) are attainable due to cooling by heavy elements (primarily by CII, CO, and Silicate grains) (Hellsten & Lin 2000), leading to the formation of cold molecular clouds (CMC's).

When the temperature of the CMC's is reduced by over two orders of magnitude from that of the WFC's, their Bonner-Ebert masses are reduced by over four orders of magnitude (cf. equation 17). Self-gravity is therefore much more important for the evolution of the CMC's than for that of the WFC's. Cloudlets close to the Bonner-Ebert mass are centrally condensed. When their mass exceeds the Bonner-Ebert mass, thermal pressure can no longer support the weight of the envelope, and the cloudlets undergo inside-out collapse (Shu 1977). During the collapse the Jean's mass decreases with the increasing density. Due to the centrally-concentrated cloud structure, however, the Jeans mass is always larger than the mass contained inside any given radius. The collapse is therefore stable, and does not lead to fragmentation in the absence

of further unstable cooling, such that the initial value of $M_{crit}$ represents the minimum mass for isothermal collapsing clouds (Tsai 1992). Numerical simulations show that even rotating centrally-concentrated clouds have difficulties in breaking up into fragments with a small fraction of $M_{crit}$ (Burkert & Bodenheimer 1996). This conjecture is in contrast to the conventional opacity-limited fragmentation scenario (Hoyle 1953; Low & Lynden-Bell 1976) which may be more appropriate for the collapse of unstable homogeneous clouds (Burkert & Bodenheimer 1993). The initial conditions required by the opacity-limited fragmentation scenario may be difficult to accomplish in nature.

In a metal-free environment, the temperature of the CFC's, $T \sim 10^2$ K and $M_{crit} \sim 10-10^2 M_\odot$. Stars formed in such a metal-poor environment are massive and short-lived, consistent with their rarity today (Hellsten & Lin 2000). The early chemical enrichment is dominated by the output of Type II supernovae, consistent with the abundance distribution observed among stars with [Fe/H]$< -1$ (Wheeler, Sneden, & Truran 1989).

The massive stars are also copious sources of UV radiation. The effect is twofold. Photons in the range 11-13.6 eV are able to penetrate clouds and photodissociate $H_2$ within them, unless their column densities are so high the clouds are self-shielded. Higher energy photons ionize and heat the gas to $10^4$ K. The loss of coolants, and increased heating means that a population of $\sim 10^5$ O5 stars is adequate to photoionize all the CMC's, re-heat them to $T \sim 10^4$ K, and prevent the formation of any additional CMC's out to a few tens of kpc. Photoionization heating also increases $M_{crit}$ to $\sim 10^6 M_\odot$, stablizing small cloudlets, and quenching star formation. As the massive stars evolve off the main sequence, the UV flux decreases, cooling again leads to $T \sim 10^2$ K in sheltered regions, and spontaneous star formation is resumed. Thus, the formation rate of massive stars may be estimated from the assumption that it is self-regulated at a level necessary to sustain marginal ionization of all WFC's. This self-regulated star formation rate naturally yields values of [Fe/H] comparable to that observed in halo stars (Lin & Murray 1992).

The rate at which massive stars must be formed is determined by the need to balance ionization with recombination in the WFC's. The mean free path for Lyman continuum photons is large in the RHG, but not in the WFC's. For sufficiently high covering factor, we can assume that a large fraction of the UV photons produced by hot stars are absorbed locally. In equilibrium then, the total production rate of UV photons per unit volume must balance the total recombination rate per unit volume. This radiative equilibrium results in high ionization in the limit

$$n_* Q_0 = n_w^2 \alpha_B \int \frac{4}{3} \pi S^3 \frac{\mathrm{d}n_c}{\mathrm{d}S} \mathrm{d}S = \left( \frac{T_h}{T_w} \right) \frac{\alpha_B}{\mu_w} \langle \rho_w \rangle, \tag{32}$$

where $n_*$ is the number density of stars, $Q_0$ is the average UV output in photons $\mathrm{s}^{-1}$ per star, and $\alpha_B$ is the case B recombination coefficient (Osterbrock 1989).

The production of UV photons is dominated by O stars, with lifetimes $\tau_* \approx 3 \times 10^6$ yr. The

average mass loss rate per unit volume from the warm phase due to star formation is then given by

$$\dot{\rho}_{SF} = \frac{n_* m_{sf}}{\tau_*} = \frac{m_{sf}}{\tau_*} \frac{\alpha_B}{Q_0} \frac{T_h}{T_w} \frac{\langle \rho_w \rangle}{\mu_w} n_h, \tag{33}$$

where $m_{sf}$ is the mass of stars that form to produce $Q_0$ photons per unit time. If the stars follow a Salpeter mass function, with a minimum mass of 0.1 $M_\odot$ and maximum mass of 100 $M_\odot$, then

$$\frac{Q_0}{m_{sf}} \approx 4 \times 10^{47} \text{photons } M_\odot^{-1} \text{ s}^{-1}. \tag{34}$$

The rate of mass depletion by star formation in the warm phase derived above is independent of the size distribution of the WFC's, and depends only upon their filling factor and internal density.

## 5. Protogalactic Models

### 5.1. The Numerical Scheme

We have performed one-dimensional Lagrangian hydrodynamic models of the evolution of the RHG subject to the physical processes discussed above. The models treat the warm and hot phases as separate fluids, evolving within a fixed external gravitational potential set by the dark matter. Angular momentum of the gas is not included. The models are applicable to the very early stages of star formation in galaxies or after mergers, or to cooling flows, before the gas has contracted sufficiently for its motion is dominated by angular momentum. During the later disk formation phase of a galaxy, or in the innermost regions of mergers or cooling flows, angular momentum would play an important role, whereas for the situations modelled here it would not strongly affect the physical processes under consideration.

The momentum equation for the RHC

$$\frac{\mathrm{d}u_h}{\mathrm{d}t} = -4\pi R^2 \frac{\partial P_h}{\partial m} - g - F_{drag}, \tag{35}$$

includes contributions from the gas pressure, $P_h$, the dark matter potential, $g$, and drag from the infalling WFC's. In equation (35), $u_h$ is the radial velocity of the RHG, and $4\pi\rho_h R^2 \mathrm{d}R = \mathrm{d}m$. For computational simplicity, the gravitational potential is taken to be isothermal out to a radius of 50 kpc, such that $g = V_c^2/R$. The magnitude of $g$ is held constant within a core radius $R_{core} = 1$ kpc and dark matter is assumed to vanish outside of 50 kpc, such that $g$ becomes Keplerian. Although this prescription of $g$ is highly simplified, our results do not depend sensitively upon the detailed form of $g$. The form of the drag term is

$$F_{drag} = \int \pi S^2 \left(V_t - u_h\right)^2 \frac{\mathrm{d}n_c}{\mathrm{d}S} \mathrm{d}S. \tag{36}$$

As noted above, in models where high mass clouds dominate, we set $V_t = V_c$, whereas equation (5) is used in models where low mass clouds dominate.

The equation of continuity for the RHG,

$$\frac{\mathrm{d}\rho_h}{\mathrm{d}t} = -\left[\frac{\rho_h}{R^2}\frac{\partial}{\partial R}\left(R^2 u_h\right) + \dot{\rho}_c(R,t)\right], \tag{37}$$

includes a sink term, due to condensation of gas out of the hot phase. The amount of mass lost from the hot phase depends upon the relative magnitudes of heating and cooling. If heating either exceeds or equals cooling in the RHG, then $\dot{\rho}_c = 0$. If cooling exceeds heating in the RHG, however, mass is transferred from the RHG to the WFC's at a rate given by

$$\dot{\rho}_c = \frac{\rho_h - \rho_{bal}}{\tau_c}, \tag{38}$$

where $\rho_{bal}$ is the density which would be required for heating to balance cooling in the hot phase. The energy equation for the RHG,

$$\frac{\mathrm{d}e_h}{\mathrm{d}t} = \frac{\Gamma - \Lambda_{brem} - \Lambda_{cond}}{\rho_h}, \tag{39}$$

includes heating by drag from the warm phase, bremsstrahlung emission, and conduction losses into the warm phase.

The warm phase is not pressure-supported in the galactic halo, and so the mean velocity of the WFC evolves as

$$\frac{\mathrm{d}u_w}{\mathrm{d}t} = -g + F_{drag}, \tag{40}$$

where the drag term is similar to that in equation (35). A maximum infall velocity of $fV_c$ is imposed upon the warm phase. As discussed above, the parameter $f$ depends upon the details of the evolution of the warm phase. In our models, we consider values of $f = 1$ and 0.1, thus examining the differences in our results for widely varying values of $f$.

The mass of the warm phase increases by mass loss from the hot phase, and decreases by mass loss due to star formation, following the prescription given in equation (33), such that

$$\frac{\mathrm{d}\langle\rho_w\rangle}{\mathrm{d}t} = \dot{\rho}_c(R) - \left[\frac{\langle\rho_w\rangle}{R^2}\frac{\partial}{\partial R}\left(R^2\langle\rho_w\rangle\right) + \dot{\rho}_{SF}\right]. \tag{41}$$

In principle, the smallest WFC's (with $S < S_{eu}$ or $S < S_{es}$) are continually being evaporated into the RHG. But, if this phase transition increases $\rho_h$ such that cooling exceeds heating in the RHG, then an appropriate amount of hot gas would precipitate to retain thermal equilibrium in the RHG. Thus, the ratio $< \rho_w > /\rho_h$ depends indirectly on the size distribution of WFC's which determines the conductive flux between the two phases.

Finally, the WFC's are assumed to be ionized and heated by the UV flux of the nearby massive stars, such that $T_w \simeq 10^4$ K. They are also assumed to be in a pressure equilibrium with

the RGH such that $n_w = n_h T_h / T_w$. Equations (35)-(41) completely describe the $\rho_h$, $T_h$, $V_h$, $V_w$, and $< \rho_w >$ distribution. From these quantities, $T_w$, $\rho_w$, as well as the heat transfer luminosity due to bremstrahlung and conduction, $L_{\rm brem}$ and $L_{\rm cond}$ can be obtained. We solve these equations numerically with a 1-D Lagrangian method (Richtmyer & Morton 1995).

The warm and hot phases are treated as separate fluids, evolving and interacting as described above. The models described below use a grid of 400 cells for both fluids, with the cell spacing increasing outwards so as to give the best resolution in the region of interest, within 100 kpc. The outer boundary is set at 2 Mpc, with a constant pressure. The large outer radius is chosen so that conditions at that boundary cannot affect the solution. Variations by factors of two in the number of cells are found to have no significant effect upon the results. The hydrodynamic equations are evolved explicitly, while the energy equation (38) is solved implicitly, allowing the use of a simple Courant timestep criterion. The models are evolved until they reach a quasi-steady state, the results of which are shown in the following sections.

### 5.2. Model 1

Using the approach outlined above, we now consider several simple models to describe the evolution of gaseous ordinary matter in the halo of large galaxies. In principle, we should concurrently consider the cosmological evolution which led to the formation of the halo. However, such an investigation would require not only a large dynamical range in dissipationless interaction among dark matter structure but also the nonlinear evolution of ordinary matter in evolving and asymmetrical potentials. A number of authors have performed simulations of systems which follow the evolution of both dissipational and dissipationless components, either in the context of galaxy collisions, or galaxy formation (see, eg. Barnes & Hernquist 1991; Gerber, Lamb, & Balsara 1996; Lamb et al. 1997; Abel et al. 1998; Steinmetz & Navarro 1997, 1999; and references therein). Such studies are generally either unable to resolve the full dynamical range present in a young galaxy, or do not include the full range of physical processes discussed above. Fortunately, we are able to examine the importance of the processes discussed in § 3 and 4 by following the standard approach in galaxy formation simulations by breaking the problem into piecemeal tasks. In contrast to the conventional simulations (eg. Yepes et al. 1997; Elizondo et al. 1999), which mainly deal with the emergence of dark matter structure and in which the star formation process is parameterized, we assume the potential is already formed and focus our attention on the microphysics of the gas.

In the first model, we take $V_c = 220$ km s$^{-1}$, and assume that $\gamma > -3$, so that the appropriate equations to use are those derived for limit in which high mass clouds dominate. For these massive clouds, the gas drag effect is relatively weak and we initially adopt $f = 1$, *i.e.* the WFC's move inward at speeds of $V_c$.

The initial conditions of the model are uniform density in the hot phase, with $n_h = 0.01$ cm$^{-3}$, giving a mass of $\sim 10^{11}$ M$_\odot$ within a radius of 50 kpc. The average density of the warm phase is

initially taken to be 0.01 times that of the hot phase. The temperature of the hot phase is initially set to $10^6$ K. We have varied the initial conditions substantially with little change in the final distribution of the hot phase.

The model was evolved for $10^9$ yr, by which time it had reached an asymptotic quasi-stationary state. While the mass of gas continues to decrease due to star formation, the density distributions of the RHC and WFC's attain asymptotic forms. These are shown in Figure 2. Figure 2a shows the final radial distributions of the density of the hot phase (solid curve), the average density of the warm phase (dashed curve), and the density of stars formed from the warm phase during the evolution (dot-dashed curve). The stellar density is calculated using the positions of stars where they are first formed. Because the stars will form on highly eccentric orbits, for which they spend most of their time near apocenter, the calculated stellar distribution should be representative of the observed distribution, after they have undergone violent relaxation (Aarseth, Lin, & Papaloizou 1988).

As can be seen from the figure, $\rho_h$ has a fairly shallow radial dependence, varying approximately as $R^{-0.9}$. The average density of the warm phase drops off somewhat more steeply, varying approximately as $R^{-1.2}$. The stellar mass density has the steepest radial dependence, varying approximately as $R^{-3}$.

Figure 2b shows the final radial distributions of the pressure (solid curve) and temperature (dashed curve) of the hot phase. At radii near 100 kpc, the temperature remains at $\sim 10^6$ K. At smaller radii, however, the increasing density of the warm phase, with the corresponding increase in the heating rate, leads to temperatures several times higher. The combination of the density gradient with the shallow temperature gradient leads to a relatively steep pressure gradient. The magnitude of $nT \approx 7 \times 10^5$ at 10 kpc and it varies approximately as $R^{-1}$. The change in slope outside of 30 kpc is related to the form of the dark matter potential used in the model, which becomes Keplerian beyond 50 kpc.

Figure 2c shows the radial dependences of the mass ratio of the warm to the hot phase (solid curve), and of the volume filling factor, $f_V$ of the WFC's (dashed curve). We define $f_V$ as $f_V \equiv \langle \rho_w \rangle / \mu_w n_w$, ie. it is the ratio of the average density of the warm gas to the internal density of the WFC's. As can be seen, most of the mass of the system is in the WFC's. It is also seen that $f_V$ shows very little variation with radius, and $f_V \approx 0.01$ for $R_c \lesssim R \lesssim 100$ kpc. The lack of variation in $f_V$ may seem somewhat counterintuitive, given that $\langle \rho_w \rangle$ decreases at larger radii. It is a consequence, however, of the fact that the WFC's are in pressure balance with the RHG, and the pressure of the latter increases rapidly towards smaller galactic radii. The clouds are therefore compressed into much smaller radii at small $R$. Note also that the ratio $\langle \rho_w \rangle / \rho_h > 1$ everywhere, such that most of the ordinary matter is in the WFC's rather than residing in the RHG. This tendency arises because $\tau_c < \tau_d$ initially in this model.

Figure 2d shows the radial dependences of the ratio of the depletion timescale of the WFC's by star formation to the dynamical timescale (solid curve), and the ratio of cooling in the RHG

by bremsstrahlung emission to that by conduction into the WFC's (dashed curve). The depletion timescale is defined as

$$\tau_{dep} = \frac{\langle \rho_w \rangle}{\dot{\rho}_{sf}}, \tag{42}$$

while the dynamical timescale

$$\tau_d = \frac{R}{V_c}. \tag{43}$$

The ratio $\tau_{dep}/\tau_d$ gives a rough estimate of the ability of the system to replenish warm gas that has been lost to star formation (it is also replaced by mass lost from the warm phase, but this can be replenished only by motions at the sound speed of the hot phase, $c_s \sim V_c$). As can be seen from the figure, both ratios are $\gg 1$ between $R_c$ and 100 kpc. Only in the inner regions of the halo, $\tau_{dep}$ becomes a significant fraction of $\tau_d$ such that efficient conversion from gas into stars is possible.

For the values of $T_h$ and $\rho_h$ in the model, most of the flux from bremsstrahlung emission is composed of X-ray photons. In the low density outer regions of the halo, bremsstrahlung is not an efficient radiative process, and a comparable amount of energy is lost to the RHG via conduction. Within 100 kpc, the total luminosity of bremsstrahlung emission is $L_{brem,Tot} = 1.2 \times 10^{11}$ L$_\odot$. By comparison, the total energy lost from the RHG via conduction into the WFC's (and immediately radiated from the WFC's) is $L_{cond,Tot} = 1.3 \times 10^{10}$ L$_\odot$. In the models discussed below, a much greater fraction of the energy is lost via conduction. Based on these results, we do not expect these systems to be luminous source of X-rays.

### 5.3. Model 2, Changes with $V_c$

We compare the results of the previous model with one having a circular velocity of 100 km s$^{-1}$. Such a model represents a dwarf system either at any epoch, or one which will become a larger system, but is at an early stage of evolution and has not yet undergone significant merging. In CDM models (Blumenthal et al. 1984; Thoul, & Weinberg 1996; Navarro, Frenk, & White 1997; Klypin, Nolthenius, & Primack 1997; Abel & Mo 1998), the first structures which form are significantly smaller than this. However, as can be seen from comparing the results below with those of Model 1, systems with significantly smaller values of V$_c$ are unlikely to contain a significant mass of RHG, and the assumptions of the models would not be applicable to such systems. The results of Model 2 are shown in Figure 3, which illustrate the same quantities as Figure 2.

In Figure 3a, it can be seen that the densities are reduced significantly relative to the model with higher $V_c$. The relative sense of the steepness is retained, though the slopes are somewhat different, with $\rho_h$ varying approximately as $R^{-2/3}$, $\langle \rho_w \rangle$ as $R^{-1.5}$ and $\rho_*$ as $R^{-2.5}$.

As shown in Figure 3b, the temperature gradient in the RHG is again very shallow. The pressure of the RHG varies approximately as $R^{-1}$, but it is lower than in the previous model, with $n_h T_h \approx 3 \times 10^4$ at 10 kpc.

The smaller value of $V_c$ relative to the previous model reduces the heating efficiency of the WFC's. In order to balance heating and cooling, the density of the RHG is reduced relative to the previous model. This reduction in the RHG's density relative to that of the warm phase is accompanied by increases in the mass ratio of the warm to the hot phase, and of the filling factor of the warm phase. Both of these quantities are larger by an order of magnitude relative to the earlier model, as can be seen in Figure 3c. We also note that within 1.5 kpc, where $f_V > 1$, our model assumptions obviously break down. In this case, the WFC's should be considered as a coherent entity rather than an assembly of smaller clouds.

The relatively small pressure of the RHG leads to low internal density of the WFC's, and a corresponding reduction in the star formation rate. This is reflected in the large values of $\tau_{dep}/\tau_d$ shown in Figure 3d. The reduced density of the RHG and the large $< \rho_w > /\rho_h$ ratio also increase the relative importance of conductive cooling of the RHG relative to bremsstrahlung emission. We find total luminosities out to 100 kpc of $L_{cond,T} = 7.2 \times 10^8$ L$_\odot$ and $L_{brem,T} = 5.1 \times 10^9$ L$_\odot$.

### 5.4. Model 3, Changes with $f$

In Figure 4, we show the results of a model in which $V_c = 220$ km s$^{-1}$, and in which $f = 0.1$, ie. the WFC's move inwards with speeds of at most $V_t = 0.1V_c$. This prescription would represent a situation in which disruption, coalescence, and coagulation occur on timescales short compared to the acceleration timescale of the clouds. Figure 4 shows the same quantities as Figure 1.

The reduction of the infall velocity has a similar affect as a relatively small $V_c$, that is, a decrease in the heating efficiency of the RHG by the WFC's, relative to the $f = 1$ case. Both density and pressure of the RHG are relatively small in this model, similar to that seen in Model 2, which has a smaller value of $V_c$. With a relatively small density, the RHG loses more energy through conduction into the WFC's than by bremsstrahlung everywhere in the system (Figure 4d). The total luminosities of the two processes are found to be $L_{cond,Tot} = 8.5 \times 10^9$ L$_\odot$ and $L_{brem,Tot} = 1.4 \times 10^8$ L$_\odot$.

The reduction in the infall velocity also leads to a shallower density profile in the WFC's. Comparing with the earlier models, this tendency causes star formation to be enhanced at large radii and suppressed at smaller radii. Consequently, the stellar density becomes relatively shallow compared with previous results.

### 5.5. Model 4, Domination by small clouds

We have also considered a model in which $\gamma < -4.5$ so that the total mass and surface area of the cloud population is dominated by the small rather than the large clouds. In this limit, heating of the RHG, and conductive losses from the RHG into the WFC's are taken from equations (24)

and (30). The infall speed of the WFC's is limited to

$$V_t = \left( D_\rho \frac{S_{es}}{R} \right)^{\frac{1}{2}} V_c. \tag{44}$$

Due to their relatively low infall velocities, individual small clouds are less efficient at heating the RHG than are large clouds. For a given $\langle \rho_w \rangle$, therefore, a distribution dominated by small clouds leads to a significantly smaller value of $G$. In addition, the larger surface-to-volume ratio of a distribution of WFC's dominated by small clouds leads to a much greater conductive cooling rate as compared to that in a distribution dominated by large clouds.

The increase in its efficiency relative to the above models means that cooling by conduction into the WFC's dominates bremsstrahlung everywhere in the RHG. The combined effects of higher cooling efficiency and lower heating efficiency lead to the depletion of the RHG and a much larger mass ratio of the WFC's to the RHG relative to the models above. The lower density in the RHG relative to earlier models leads directly to smaller pressures, causing a reduction in both $n_w$ and the star formation rate. The change was so dramatic that we found $f_V > 1$, ie. the RHG effectively does not exist in the system. But, in the absence of RHG, the WFC's cannot fragment through Kelvin-Helmholz instability to offset their growth through cohesive collisions (see §3.3). Thus, the large $< \rho_w > / \rho_h$ ratio and the dominance of the small clouds appears to be incompatible. A self-consistent treatment of both phases, including the size distribution of the WFC's will be examined and discussed in a future paper.

The above models assume that $\Lambda_w = 10^{-22}$ergs cm$^3$ s$^{-1}$, a high value for warm clouds, near that of the peak from hydrogen emission. Such would be expected, given the stability arguments presented in § 3, if the small cloud population is dominated by those clouds which are just able to radiate away the energy conducted into them from the RHG. If, however, the small cloud population is dominated by slightly larger clouds, which can radiate more efficiently, then a much small value of $\Lambda_w$ may be more appropriate. We have therefore repeated Model 4 using $\Lambda_w = 10^{-24}$ergs cm$^3$ s$^{-1}$. The decreased emission efficiency of the small clouds led to results that were significantly different from those found above, and closely resembled those found for Model 3. The difference between these two possible cases remains an uncertainty in this work, and shall be resolved in upcoming models which examine the structure of WFC's embedded within the RHG.

## 6. Discussion

In this paper, we examine the microphysics of gas dynamics in the early epoch of galactic evolution. Our objective is to provide a description of the dominant physical processes in ordinary matter which may be applied to a large class of galaxy formation models. For example, in the canonical hierarchical galaxy formation scenario, small dwarf-galaxy building blocks, containing non-interactive dark matter and gaseous ordinary matter, form first and subsequently merge to

form larger entities such as our Galaxy. In the present analysis, we neglect the dynamical evolution of the dark matter halo which is undoubtedly important in determining not only the formation process but also the present kinematic properties of galaxies. This approximation enables us to focus our attention upon the evolution of gas in the early epoch of galactic evolution, which regulates the rate and location of star formation and therefore the light distribution and chemical properties of the emerging galaxies. We discuss below three possible applications of our results.

### 6.1. Galactic Stellar halo

The results presented here show that thermal instability results in the formation of the residual halo gas (RHG), with density and pressure appropriate for quasi-hydrostatic and energy equilibria, and warm fragmentary clouds (WFC's), which are pressure confined by RHG and heated by ionizing UV photons. Such systems have been proposed as being the source of observed Lyman-limit systems (Mo & Miralda-Escude 1996). The mass limits of the WFC's are set by the same criteria as in the earlier work, but in this work we include many more details of the interactions between the phases.

Inside $\sim 10 - 100$ kpc, WFC's in galaxies with masses comparable to the Galaxy are self-shielded from the extragalactic UV flux (see Figure 1). Unless these WFC's are continually heated by the UV flux from nearby massive stars, further cooling reduces their temperature to $\leq 10^2$ K. Gravitational instability in the large WFC's leads to spontaneous formation of stars among which the massive stars radiate UV photons, ionize their surroundings, and quench the formation of additional stars during their lifetime (Lin & Murray 1992). Through such a self-regulating feedback process, the maximum rate at which gas may be converted into stars is determined by the maintenance of an adequate UV flux to photoionize all the WFC's (§4.2).

In the regions far from the center of the halo where the density of the RHG is relatively low, the internal density of the WFC's and their average density $< \rho_w >$ are also low. The effect of self-regulation limits the star formation timescale $\langle \rho_w \rangle / \dot{\rho}_{SF} > \tau_d$. But, the star formation efficiency is much higher at smaller galactic distances. The results in Figures 2-4 show that within a few kpc (depending on the model), the stellar density $\rho_*$ already exceeds both $< \rho_w >$ and $\rho_h$ after 1 Gyr. Once the stars are formed out of gas, they cannot dissipate their orbital energy such that their orbital radii cannot contract further. Thus, the interaction between RHG, WFC's, and the newly formed massive stars essentially determines the asymptotic surface brightness distribution in galaxies. In Figure 5, we show the computed surface density profiles computed from the stellar distributions of Models 1-3. As can be seen, the models are fairly well fit by deVaucouleur profiles within the inner 50 kpc, in good agreement with the profiles of spheroidal systems.

The onset of rapid and efficient star formation invalidates the instantaneous mixing and incremental gas-to-star conversion assumptions which are essential to the closed-box models for galactic chemical evolution and enrichment (cf Binney & Tremaine 1987), despite the apparent

consistency between it and the observed metalicity distribution among population II stars (Chiappini et al. 1999). If these stars are formed in a series of starburst events in which a large fraction of the remaining gas is converted into stars on a timescale shorter than the dynamical timescale of the galaxy or the lifespan of the massive stars, the metallicity distribution would reflect the metallicity inhomogeneity in WFC's. In this case, the deficiency of extremely metal poor stars (with [Fe/H]$\lesssim$-3) would be consistent with an evolving initial mass function which gradually becomes less biased towards massive stars as the WFC's are chemically enriched.

A necessary condition for the formation of stars with long-lived, low-mass stars is small $M_{crit}$ (see §4.2). In a self-regulated environment, WFC's with [Fe/H]$\gtrsim$-3 can spontaneously cool from $10^4$ K to $\sim 10$ K (so that $M_{crit} \lesssim 1 M_\odot$) between successive generations of nearby massive stars (with an interval $\sim$ a few $10^6$ yr) provided the initial $n_w > 0.1 - 1$ (Hellsten & Lin 2000). The corresponding external pressure needed to confine such WFC's is $nT \sim 10^{3-4}$. In Figures 2-4, we see that these values of $n_h T_h$ are attained outside 10 kpc, similar to the regions where the metal poor population II stars are located.

In the above scenario, we have neglected the effect of magnetic fields which stablize cold clouds against gravitational instability through field-ion coupling and ion-neutral collisions (cf Shu 1985; Shu, Adams, & Lizano 1993). In dense cores of molecular clouds around the solar neighborhood, low-level ionization is maintained through cosmic ray heating and the field strength declines through ambipolar diffusion (Spitzer 1978; Shu 1985). If this process is important in WFC's, the star formation rate would be much reduced from those illustrated in Figures 2-4. Collisions between WFC's would occur at velocities in excess of 10 km s$^{-1}$. Shock compression and rapid cooling near the collision interface could lead to a rapid expulsion of magnetic field, rendering its support ineffective. In the models discussed above, the covering factor of large WFC's is of order unity. A large cloud would therefore collide with another large cloud only about once during a galactic crossing time. Collisions between large and small clouds would, however, occur much more frequently. In the limit that the size distribution of the clouds is dominated by relatively small clouds, the area covering factor is large, and small clouds collide with each other much more frequently. These issues are beyond the scope of the present investigation and they need to be thoroughly investigated in the future.

### 6.2. Formation of globular clusters

The analysis presented here can also be applied to the formation of Galactic globular clusters (Lin & Murray 1996). Prior to the conversion of ordinary matter from gas into stars, the progenitors of these clusters were protocluster clouds (PCC's). The chemical homogeneities within individual clusters and the large metallicity variation among different clusters suggest that PCC's are a distinct entities which must be confined either by their own self-gravity or external pressure. But, if PCC's are entirely bound by their own self-gravity, external UV heating would not be adequate to suppress thermal instability within them (see §3.3).

The magnitude of $M_{crit}$ for the WFC's is comparable to the mass of globular clusters. We identify these warm, marginally self-gravitating and partially pressure-confined WFC's as PCC's. At Galactic distances $D \sim 3 - 30$ kpc, PCC's with mass $(M) < M_{crit}(\sim 10^6 M_\odot)$ are confined by the the pressure of the RHG, $n_h T_h \sim 10^{3-5}$, depending on the Galactic halo structure during the epoch of cluster formation (Figs. 2-4). If these PCC's are completely ionized and have a $T_w \sim 10^4$, then $n_w \sim 0.1 - 10$ cm$^{-3}$. For these structural parameters, the UV flux needed is equivalent to that emitted by a few O5 stars at a distance comparable to or greater than their size (typical a few pc) (see Figure 1). (These stars could also reside within the PCC's). These clouds could persist for a significant fraction of $\tau_d$ if the accretion of smaller clouds or condensation from the RHG is adequate to compensate for their mass loss due to stripping by the RHG.

On the observational side, in order to verify that the PCC's were pressure-confined, we first estimate their $n_w T_w$ from the current properties of globular clusters, averaged over their half-mass radii ($r_h$) (Murray & Lin 1996). We use these quantities because the stellar density and the velocity dispersion at $r_h$ do not change significantly during post-formation evolution. Extrapolation to the stage prior to star formation is, however, highly uncertain. If, after their formation, the young stellar objects undergo collapse and virialization from rest, the clouds' initial radii ($r_i$) would be $\sim 2r_h$. Larger $r_i$ would be expected if star formation requires dissipative collisions and coagulation of substellar fragments (Murray & Lin 1996). But $r_i$ is unlikely to be larger than the tidal radii of the PCC's, which are typically a few times larger than $r_h$. Thus, the initial density of the PCC's may be 1-3 orders of magnitude smaller than the average cluster density at $r_h$ today. Based on the present velocity dispersion of the clusters, we infer the initial temperature of the PCC's to be $\sim 10^4$ K, comparable to that expected if they were photoionized. From these estimates, we infer $n_w T_w \sim 10^{2-5}$ (Murray & Lin 1992). The dependence of the pressure upon galactic radius, $D$, is very poorly determined from the observational parameters. Of more significance is that the magnitude of the pressure inferred from the observations is very similar to that found in the RHG in our models (Figs. 2-4).

From these results, and the cluster metallicities, we can also estimate the cooling time scale ($\tau_{cc}$) and dynamical time scale ($\tau_{dc}$), of the PCC's. The ratio $\tau_{cc}/\tau_{cd}$ increases from $\sim 10^{-4}$ near the Galactic bulge to $\sim 1$ at $\sim 100$ kpc. In most PCC's, $\tau_{cc} << \tau_{cd}$ and thermal equilibrium is only possible in the presence of external UV photons with a flux comparable to that required by self-regulated star formation in the halo.

### 6.3. X-ray Luminosity

In the hierarchical galaxy formation process, coalescence of small stellar systems (dwarf galaxies) occurs within a few dynamical timescales. If the ordinary matter contained initially within these building blocks is to be heated through shock dissipation to the virial temperature of the common halo, the mergers would become luminous X-ray sources (Eke, Navarro, & Frenk 1998). But the results of our models indicate that; 1) thermal instability leads to the formation

of WFC's which contain most of the ordinary matter, and 2) even in the RHG, conduction may be a more efficient channel of heat loss than bremsstrahlung emission. As discussed in § 5.2-5.4, the resulting x-ray luminosities are small, ranging from $10^{11}$ $L_\odot$ in Model 1 to $10^8$ $L_\odot$ in Model 3. The spectra of the models are shown in Figure 6. The spectra of the low luminosity systems may be modified somewhat by supernova emission. Using the total star formation rates of Models 1-3, we estimate supernova luminosities of $10^{10}$ $L_\odot$ for Model 1, $6\times10^9$ $L_\odot$ for Model 2, and $5\times10^8$ $L_\odot$ for Model 3. Based upon these results, we expect relatively little X-ray luminosity to be released from regions with ongoing galaxy merging events, consistent with x-ray observations (Fabbiano & Schweizer 1995; Read & Ponman 1998).

### 6.4. Limitations

In our first attempt to investigate the complex physics of multi phase gas dynamics during the early epoch of galaxy formation, we have adopted various simplifying assumptions such as 1-D spherical symmetry and power-law size distribution for WFC's. These treatments can be improved with a self-consistent analysis of the WFC's evolution which will be presented in a follow up paper. We have also neglected the evolution of dark matter which dominates the potential. The results in Figs 2-4 show that the distribution of pressure, density, filling factor of WFC's and the star formation rate depend, though not sensitively on the potential. A full study of this problem will require the use of multi-dimensional integrated simulations of both dark and ordinary matter. While such work has been done in a cosmological context, the extreme temperature range spanned by the gas within an individual galaxy (at least four orders of magnitude) places severe demands upon a code to be able to resolve structures over many orders of magnitude in size. Our basic approach and the prescription provided here can be readily used in such investigations as they begin to be made.

We thank Drs. A. Burkert, S. Faber, U. Hellsten, C. Frenk and A. Wolfe for valuable conversations. This research has been supported in part by the NSF through grant AST-9618548 and by NASA through an astrophysics theory program grant which supports a joint Center for Star Formation Studies at NASA-Ames Research Center, UC Berkeley, and UC Santa Cruz. This work was performed in part under the auspices of the U.S. Department of Energy by the University of California Lawrence Livermore National Laboratory under contract No. W-7405-Eng-48.

## REFERENCES

Aarseth, S. J., Lin, D. N. C., & Papaloizou, J. C. B. 1988, ApJ, 324, 288

Abel, T., Anninos, P., Norman, M. L., & Zhang, Y 1998, ApJ, 508, 518

Abel, T., & Mo, H. J. 1998, ApJL, 494, L151

Barnes, J. E., & Hernquist, L. E. 1991, ApJL, 370, L65

Binney, J. 1977, ApJ, 215, 483

Binney, J., & Tremaine S. 1987, Galactic Dynamics (Princeton University Press, Princeton)

Blumenthal, G. R., Faber, S. M., Primack, J. R., & Rees, M. J. 1984, *Nature*, 311, 517

Bonner, W. B. 1956, MNRAS, 116, 356

Burkert, A., & Bodenheimer, P. 1993, MNRAS, 264, 798

—— 1996, MNRAS, 280, 1190

Burkert, A., & Lin, D. N. C. 2000, ApJ, in press

Chiappini, C., Matteucci, F., Beers, T. C., & Nomoto, K. 1999, ApJ, 515, 226

Dalgarno, A., & McCray, R. A. 1972, ARAA, 10, 375

Ebert, R. 1955, *Zs. Ap.*, 37, 217

Eke, V. R., Navarro, J. F., & Frenk, C. S. 1998, ApJ, 503, 569

Elizondo, D. Yepes, G., Kates, R., Müller, V., & Klypin, A. 1999, ApJ, 515, 525

Fabbiano, G. & Schweizer, F. 1995, ApJ, 447, 572

Fall, S. M., & Rees, M. J. 1985, ApJ, 298, 18

Ferland, G. J. 1991, OSU Internal Rep. 91-01

Field, G. B. 1965, ApJ, 142, 531

Gerber, R. A., Lamb, S. A., & Balsara, D. S. 1996, MNRAS, 278, 345

Gould, R. J., & Thakur, R. K. 1970, *Annals Phys.*, 61, 351

Haardt, F., & Madau, P. 1996, ApJ, 461, 20

Haiman, Z., Abel, T., & Rees, M. J. 2000, ApJ, in press

Haiman, Z., Rees, M. J., & Loeb, A. 1997, ApJ, 476, 458

Hellsten, U., & Lin, D. N. C. 1999, ApJ, submitted

Hollenbach, D., & McKee, C. F. 1979, ApJS, 41, 555

Hoyle, F. 1953, ApJ, 118, 513

Kepner, J. V., Babul, A., & Spergel, D. N. 1997, ApJ, 487, 61

Klypin, A., Nolthenius, R., & Primack, J. 1997, ApJ, 474, 533

Lamb, S. A., Gerber, R. A., Rudnick, G. H., & Dewing, M. 1997, *RevMexAA*, 6, 151

Lin, D. N. C., & Murray, S. D. 1992, ApJ, 394, 523

—— 1996, in Dynamical Evolution of Star Clusters: Confrontation of Theory and Observations, ed. P. Hut & J. Makino (Dordrecht: Kluwer), 283

Low, C., & Lynden-Bell, D. 1976, MNRAS, 176, 367

McKee, C. F., & Cowie, L. L. 1977, ApJ, 215, 213

Murray, S. D., & Lin, D. N. C. 1990, ApJ, 363, 50

—— 1992, ApJ, 400, 265

—— 1996, ApJ, 467, 728

Murray, S. D., White, S. D. M., Blondin, J. M., & Lin, D. N. C. 1993, ApJ, 407, 588

Navarro, J. F., Frenk, C. S. & White, S. D. M. 1997, ApJ, 490, 493

Osterbrock, D. E. O. 1989, Astrophysics of Gaseous Nebulae and Active Galactic Nuclei (Mill Valley: University Science Books)

Read, A. M. & Ponman, T. J. 1998, MNRAS, 297, 143

Rees, M. J., & Ostriker, J. P. 1977, MNRAS, 179, 541

Richtmyer, R. D., & Morton, K. W. 1995, Difference Methods for Initial Value Problems (Melbourne: Krieger)

Rosner, R., & Tucker, W. H. 1989, ApJ, 338, 761

Scalo, J. M. 1985, in *Protostars and Planets II*, eds. D.C. Black & M. Matthews, (Univ. of Arizona Press), 201

Shu, F. 1977, ApJ, 214, 488

Shu, F. H. 1985 in The Milky Way Galaxy (Dordrecht: Reidel), 566

Shu, F. H., Adams, F. C. & Lizano S. 1993, ARAA, 25, 23

Spitzer, L. 1956, Physics of Fully Ionized Gases (New York: Interscience)

Spitzer, L. 1978, Physical Processes in the Interstellar Medium (New York: Wiley)

Steinmetz, M., & Navarro, J. F. 1997, ApJ, 478, 13

—— 1999, ApJ, 513, 555

Thoul, A. A., & Weinberg, D. H. 1996, ApJ, 465, 608

Tsai, J. C. 1992, PhD thesis, MIT

Wheeler, J. C., Sneden, C., & Truran, J. W. 1989, ARAA, 27, 279

White, S. D. M., & Rees, M. J. 1978, MNRAS, 183, 341

Yepes, G., Kates, R., Khokhlov, A, & Klypin, A. 1997, MNRAS, 284, 235

Zinnecker, H., McCaughrean, M., J., & Wilking, B. A. 1993, in Protostars and Planets III, ed. E. H. Levy, & J. I. Lunine, (Tucson: Univ. of Arizona Press), 429

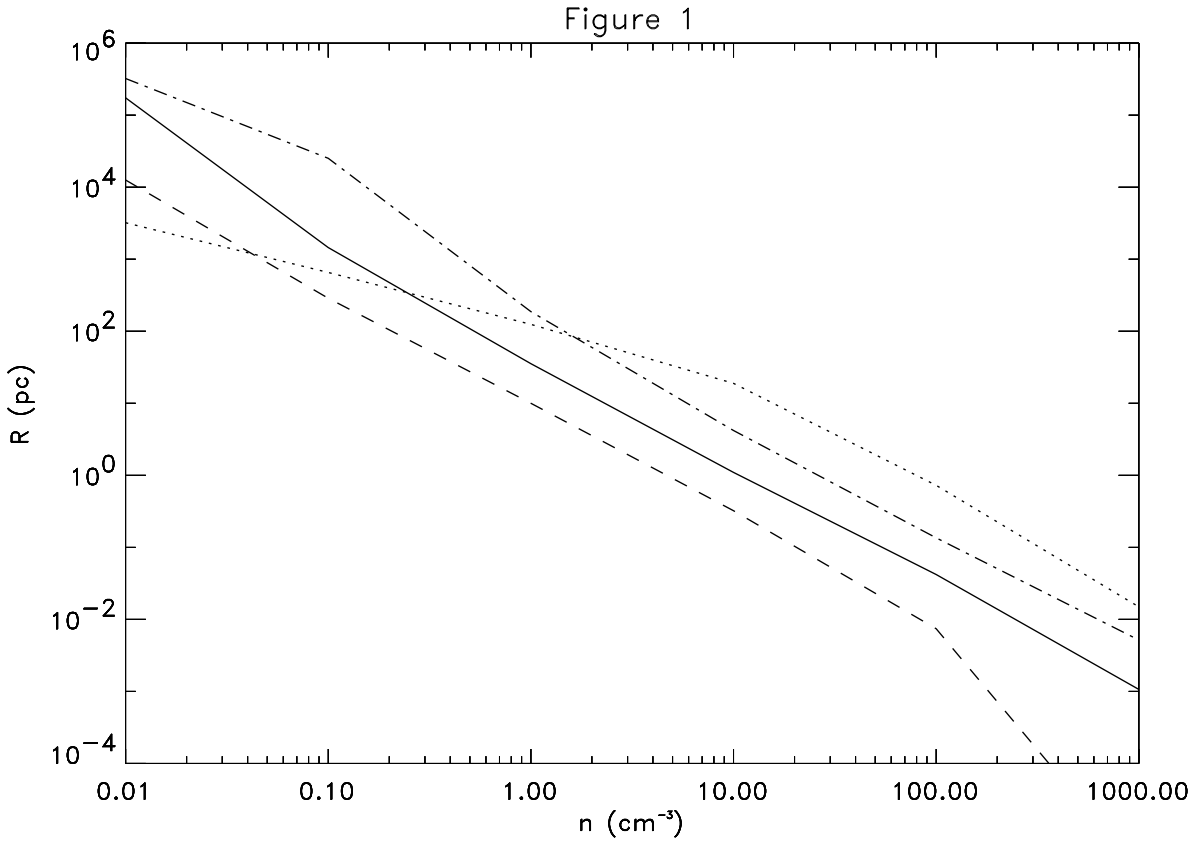


Fig. 1.— The depth into which a cloud may be ionized by various UV sources, calculated using CLOUDY. The solid, dashed, and dot-dashed curves are computed using the standard AGN spectrum of CLOUDY. The solid curve corresponds to a flux of $0.5\times10^{-21}$ ergs cm$^{-2}$ s$^{-1}$ Hz$^{-1}$ Sr$^{-1}$ at 13.6 eV, while the dot-dashed and dashed curves correspond, respectively, to fluxes larger and smaller by an order of magnitude. The dotted curve is computed using a Kurucz spectrum, with the UV flux set to correspond to that of an O5 star at a distance of 10 pc.

Figure 2

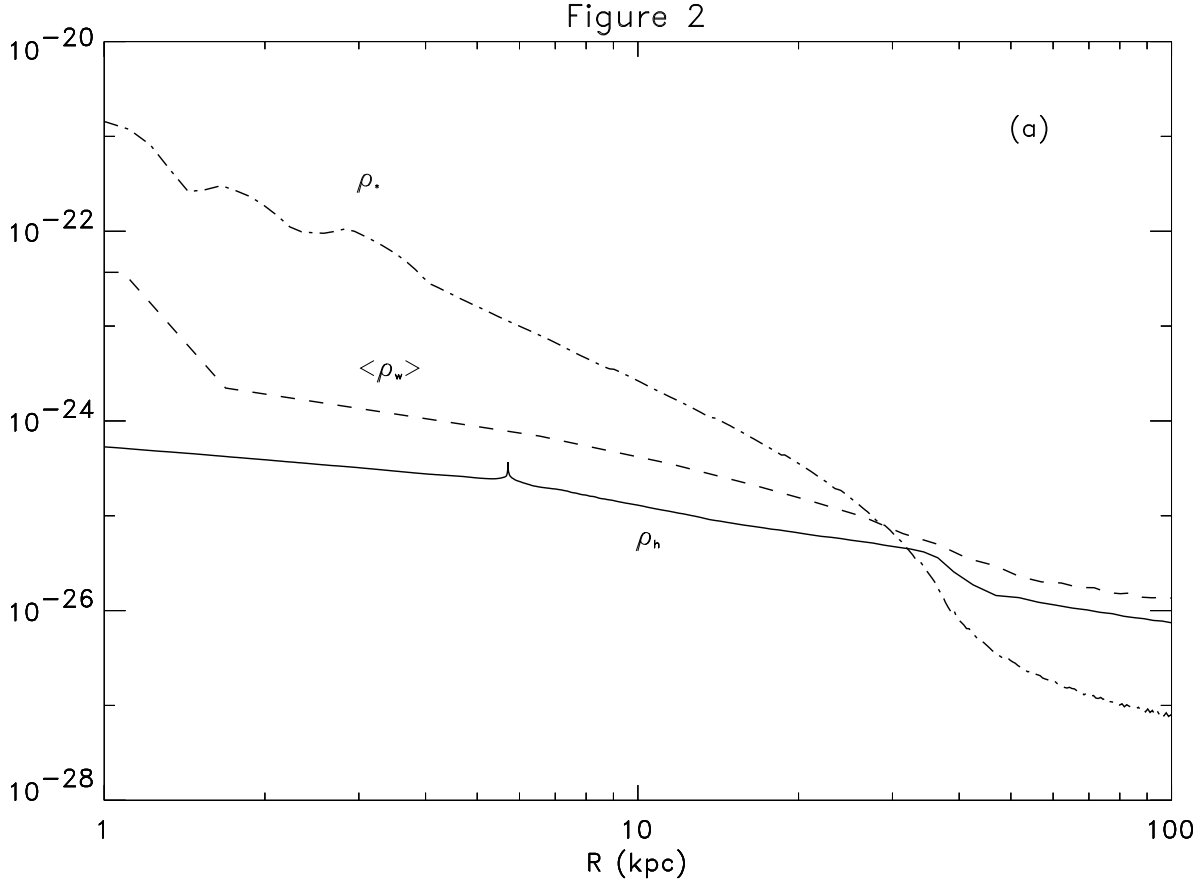

Figure 2

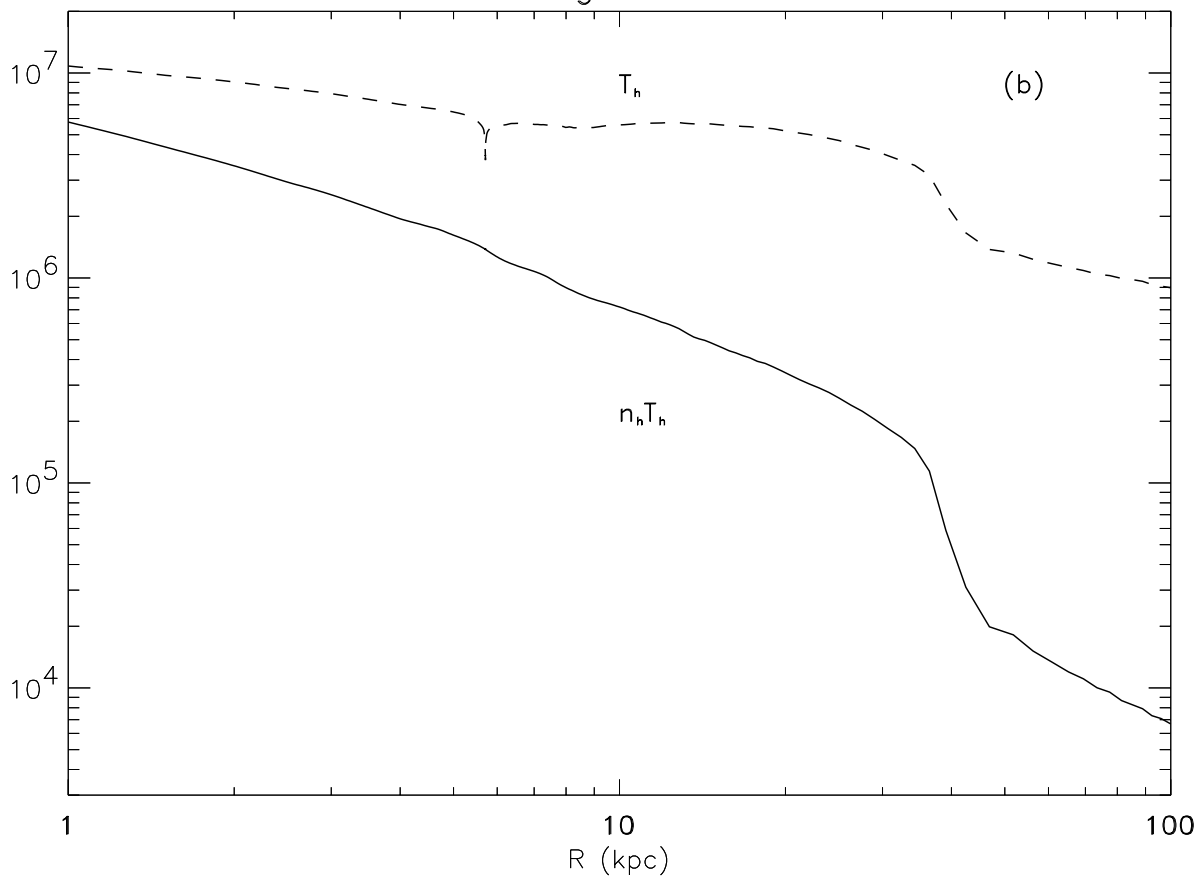

Figure 2

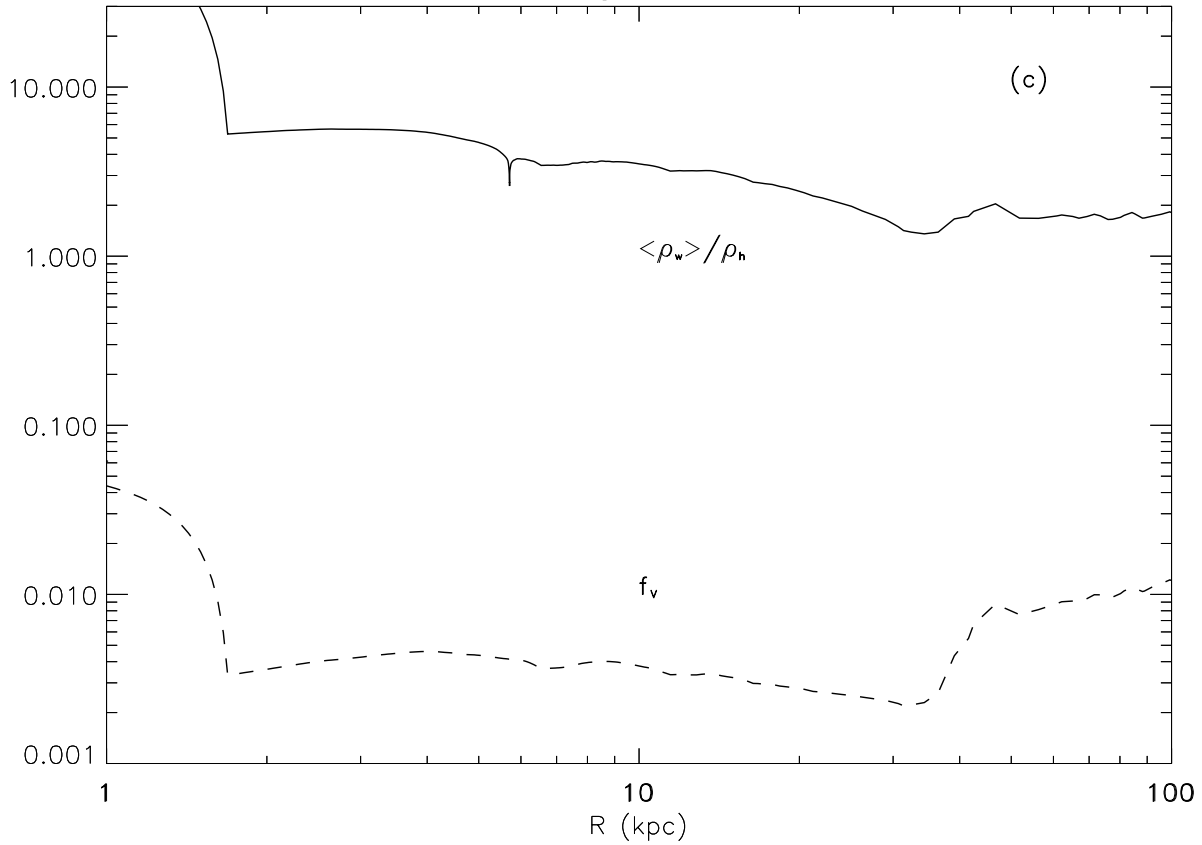

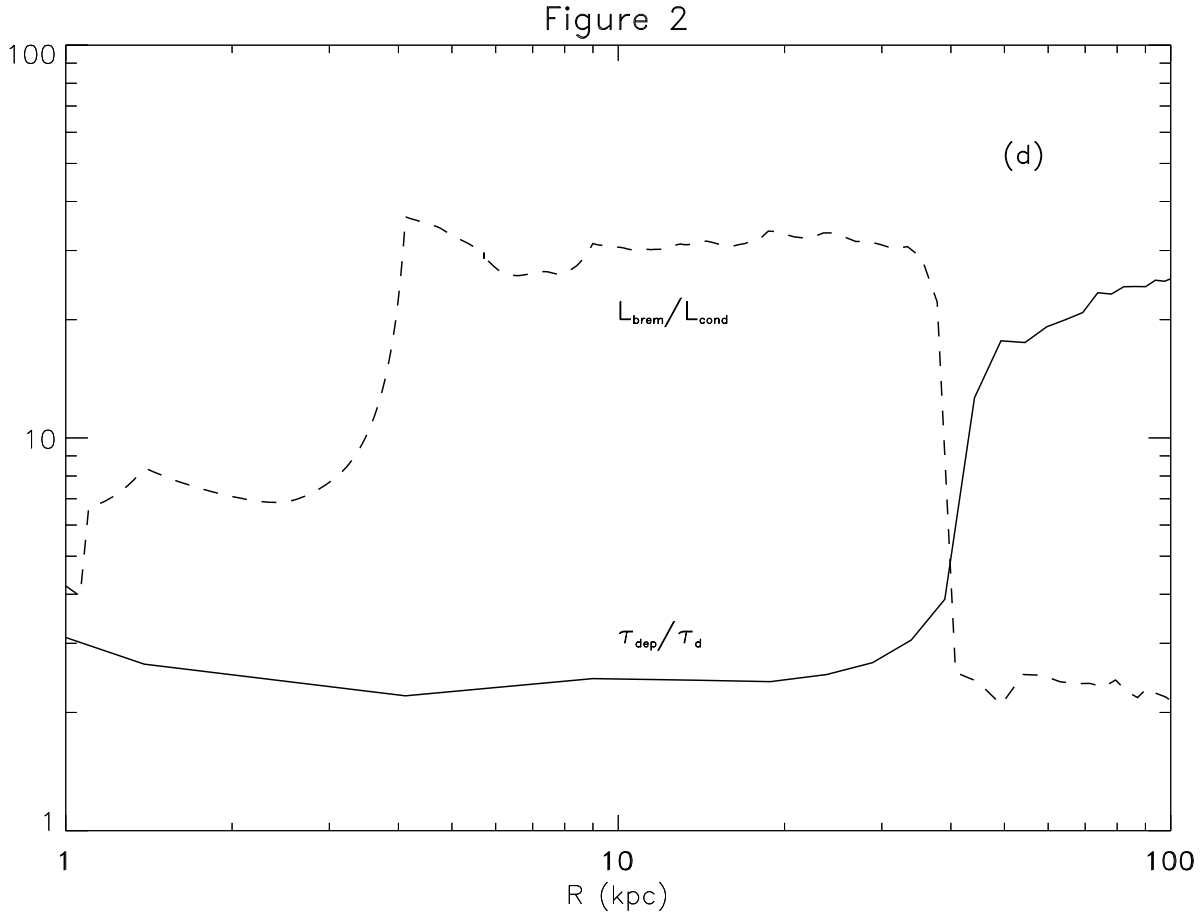


Fig. 2.— Model 1 at $10^9$ yr. In (a) are shown the density of hot gas (solid), the average density of the warm gas (dashed), and the stellar mass density (dot-dashed). In (b) are shown the temperature (dashed) and pressure (solid) of the hot phase. In (c) are shown the mass ratio of the warm and hot phases (solid) and the volume filling factor of the warm clouds (dashed). In (d) are shown the ratio of the depletion timescale to the dynamical timescale (solid) and the ratio of the efficiency of cooling of the hot phase by bremsstrahlung emission to that by conduction into the cool clouds (dashed). All quantities are shown as functions of galactic radius.

Figure 3

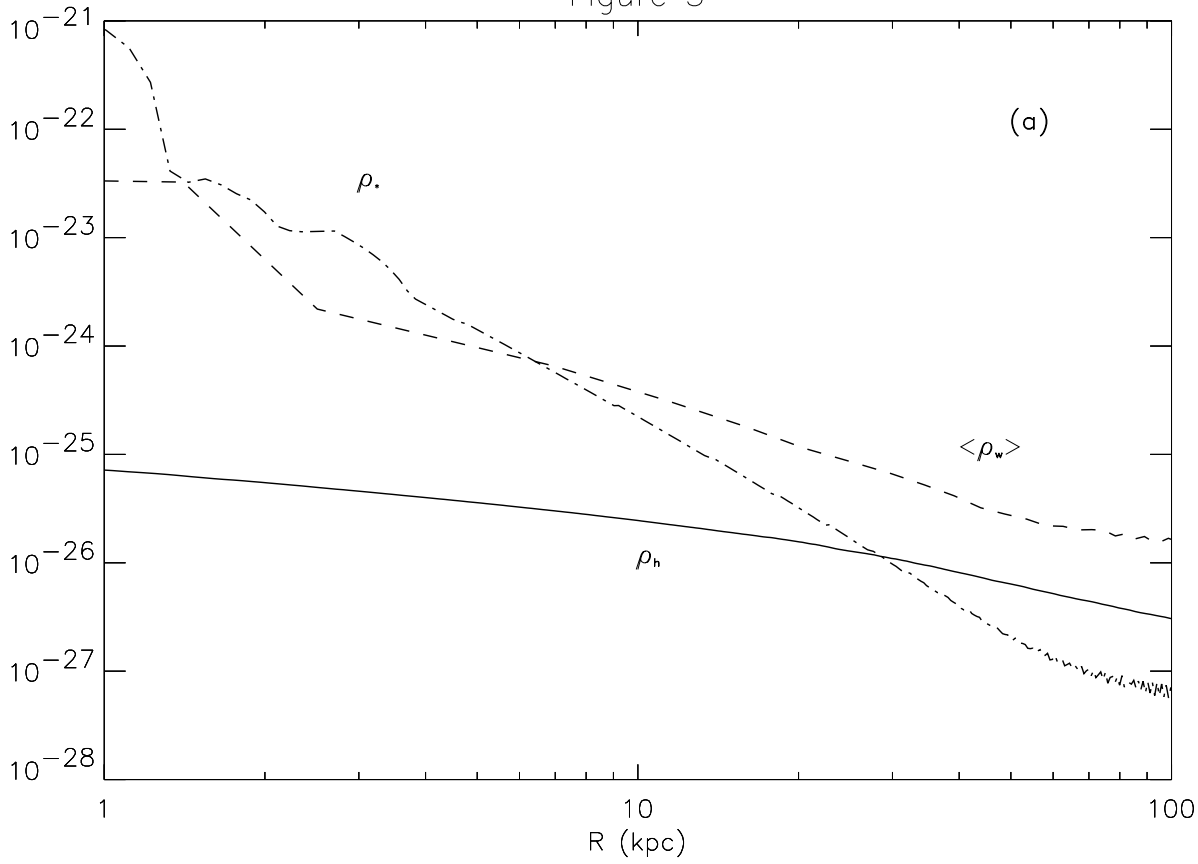
$10^{-21}$
$10^{-22}$
$10^{-23}$
$10^{-24}$
$10^{-25}$
$10^{-26}$
$10^{-27}$
$10^{-28}$
(a)
$\rho_*$
$<\rho_w>$
$\rho_h$
1
10
100
R (kpc)

Figure 3

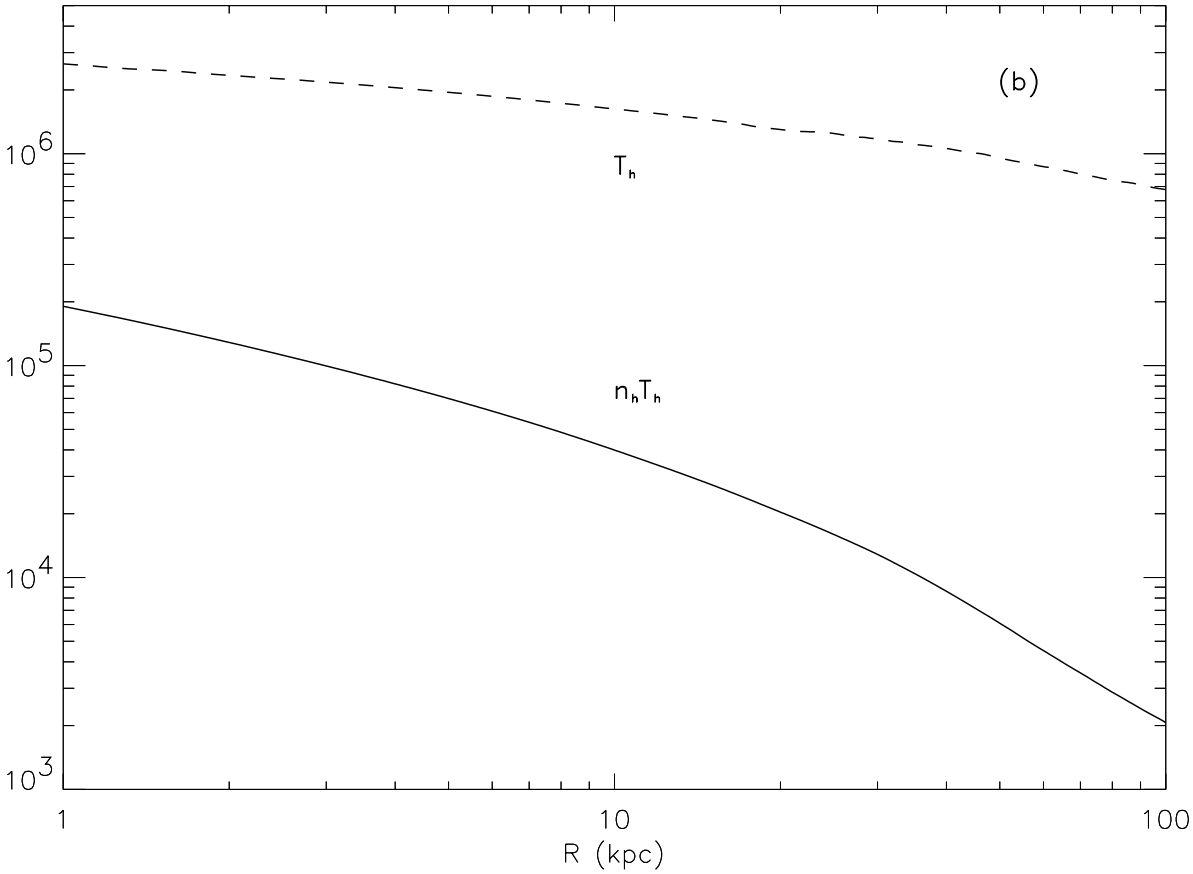

Figure 3

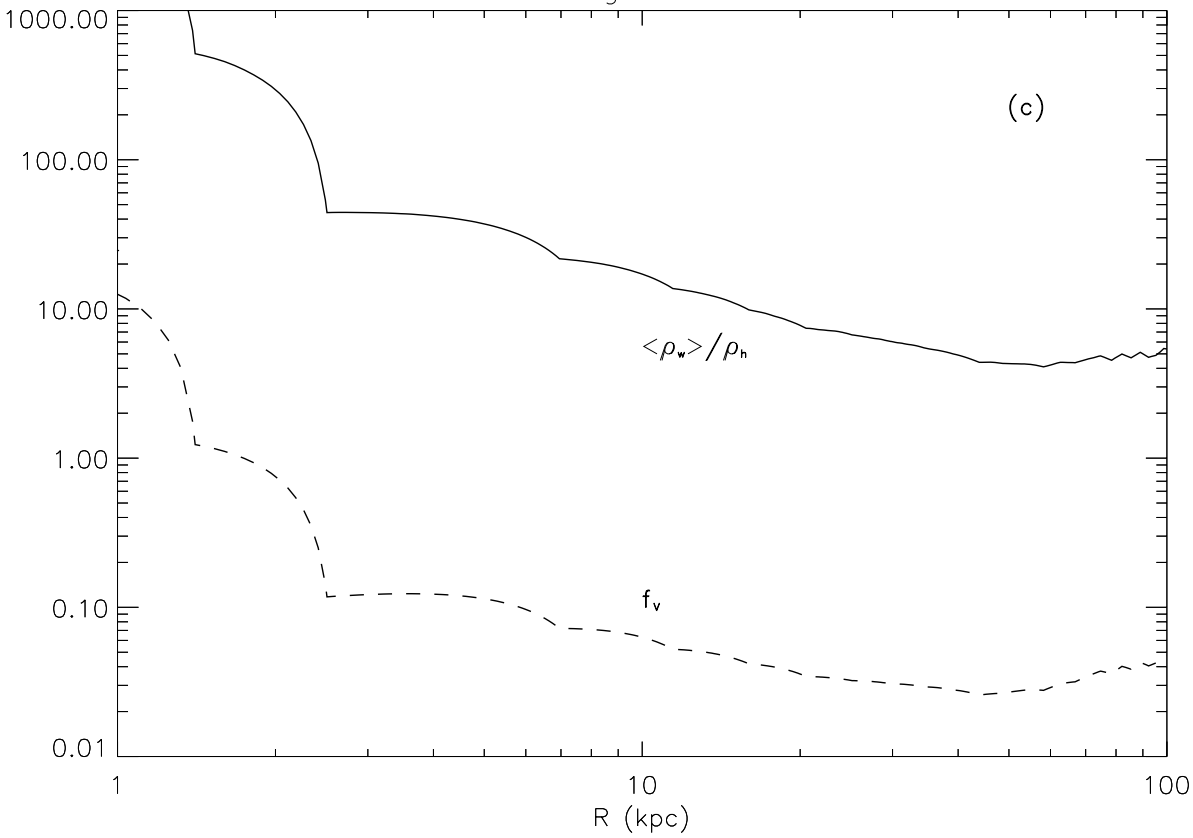

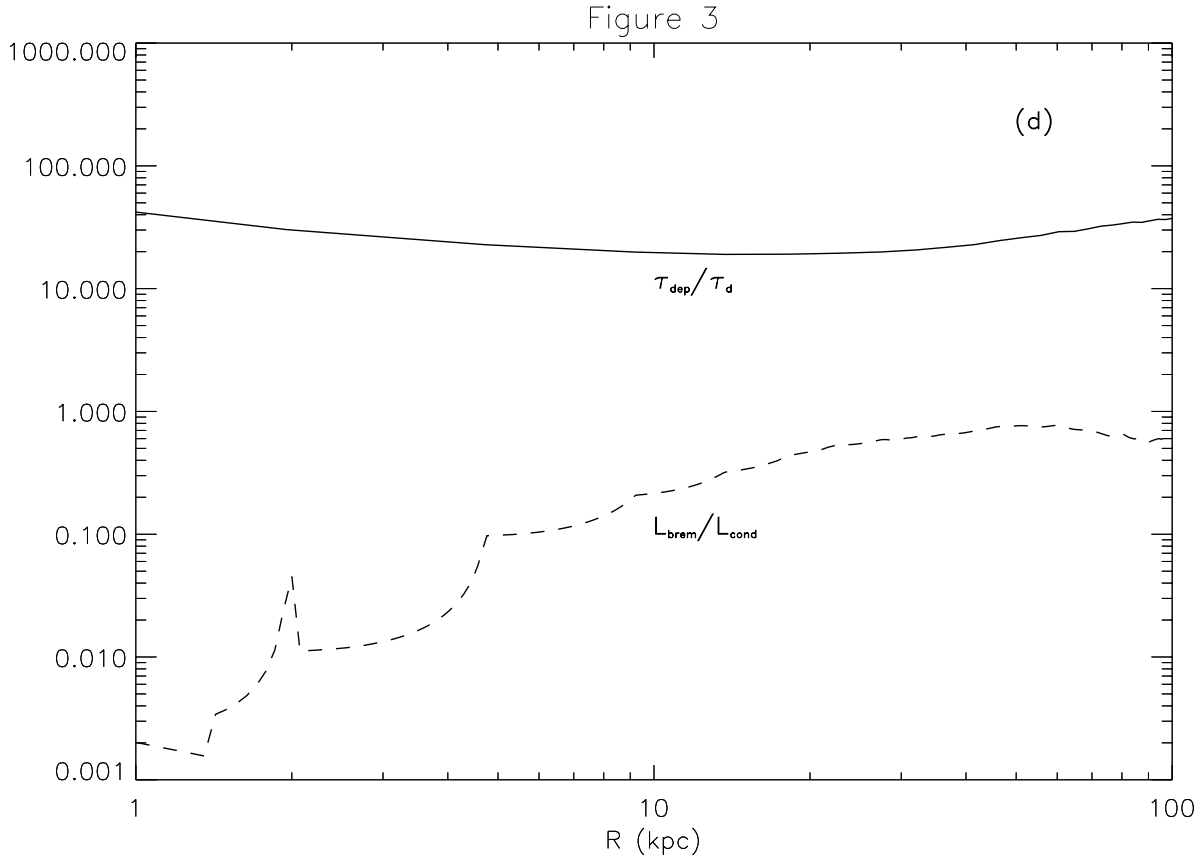


Fig. 3.— Model 2 with $V_c = 100$ km s$^{-1}$ at $10^9$ yr, displayed as in Figure 2. With a lower circular speed, the heating of the RHG by motions of the WFC's is reduced relative to that of Model 1. As compared to Model 1, Model 2 has similar mean density of the warm gas, whereas the density of the RHG is reduced by approximately an order of magnitude. The filling factor of the warm clouds is thus about an order of magnitude greater than in Model 1. The reduced pressures relative to Model 1 lead to lower density within the WFC's, reducing the star formation rate necessary to maintain the warm phase, and so the stellar density is also reduced relative to Model 1. The low density of the RHG relative to Model 1 also leads to conduction into the WFC's losses playing a dominant role in energy loss from the RHG, contrary to the case in Model 1.

Figure 4

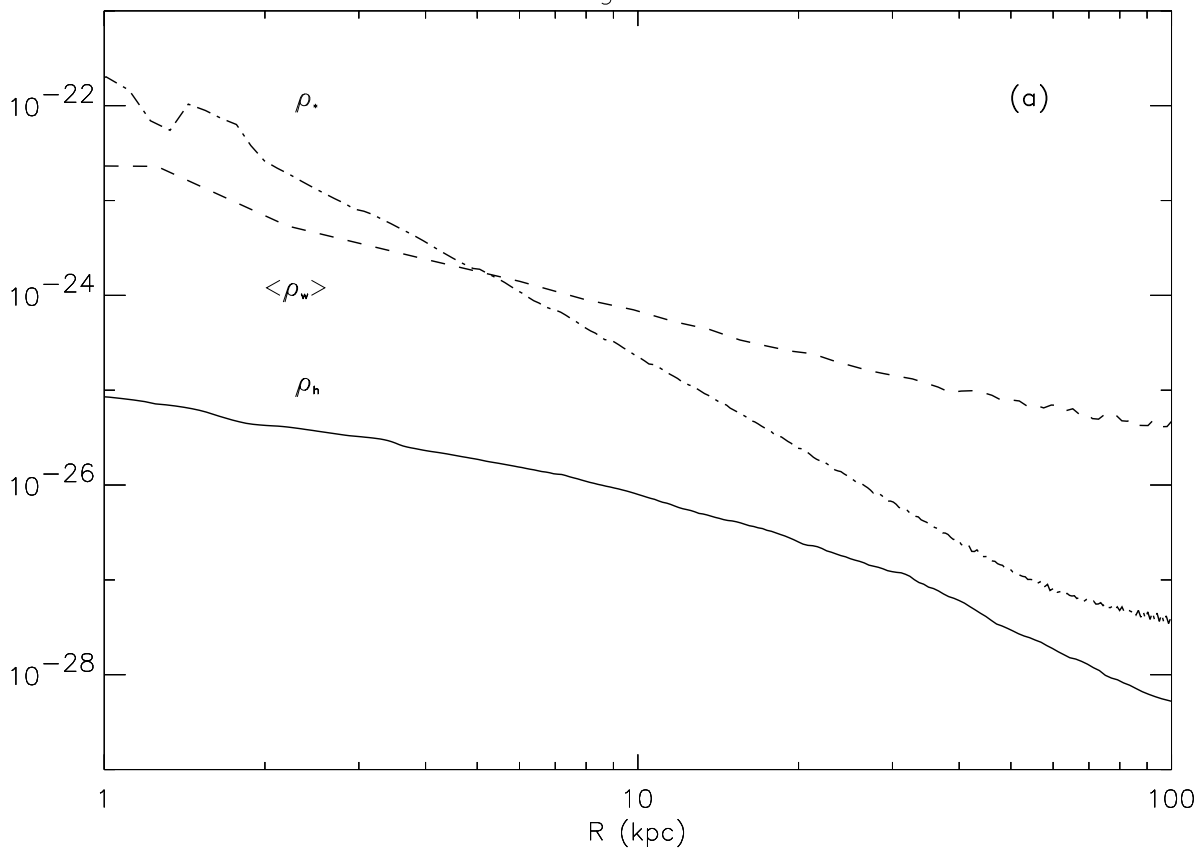

Figure 4

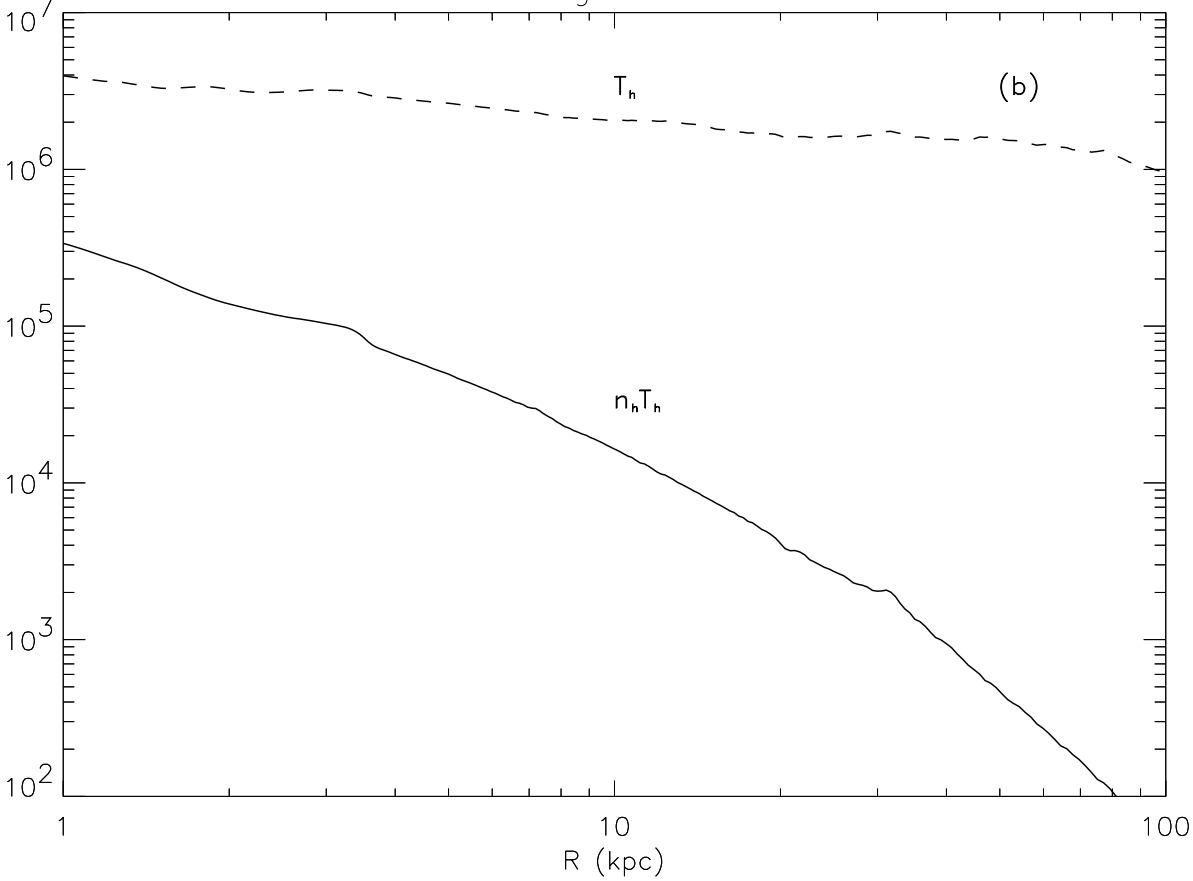

Figure 4

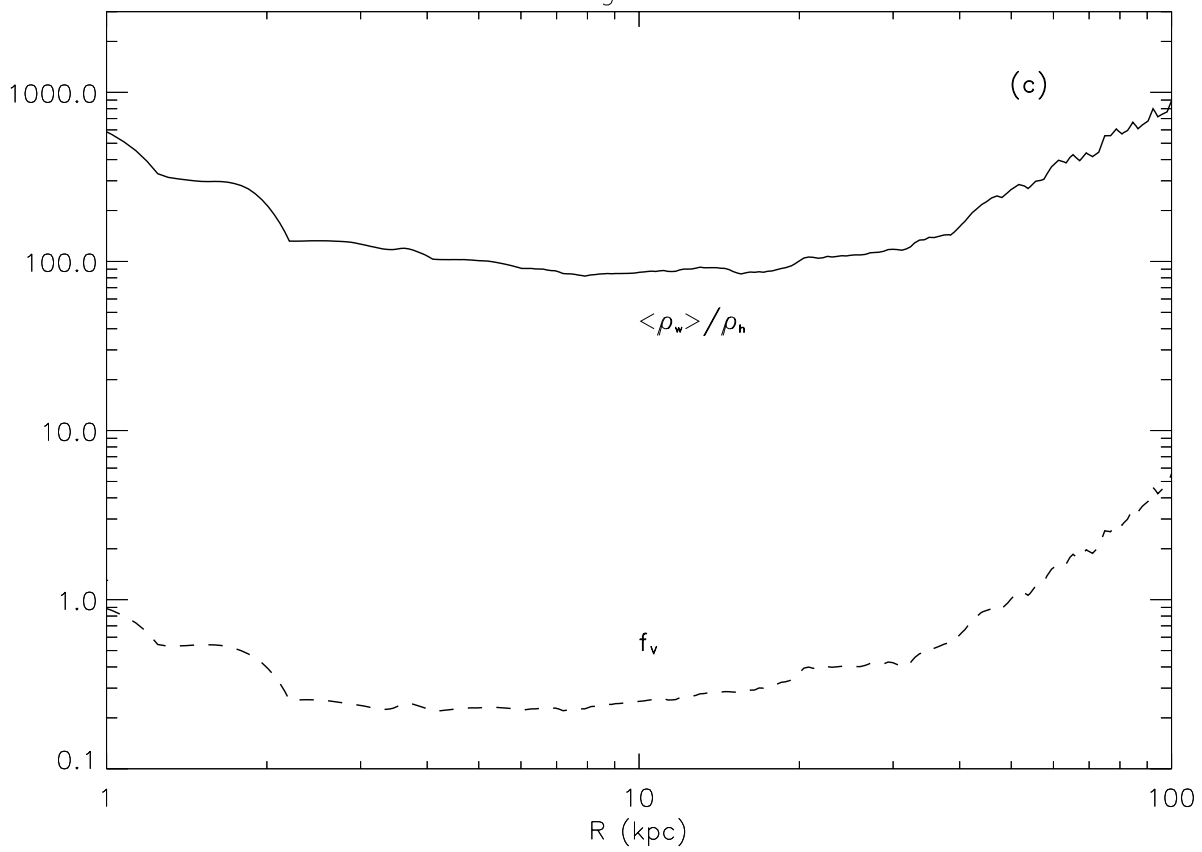

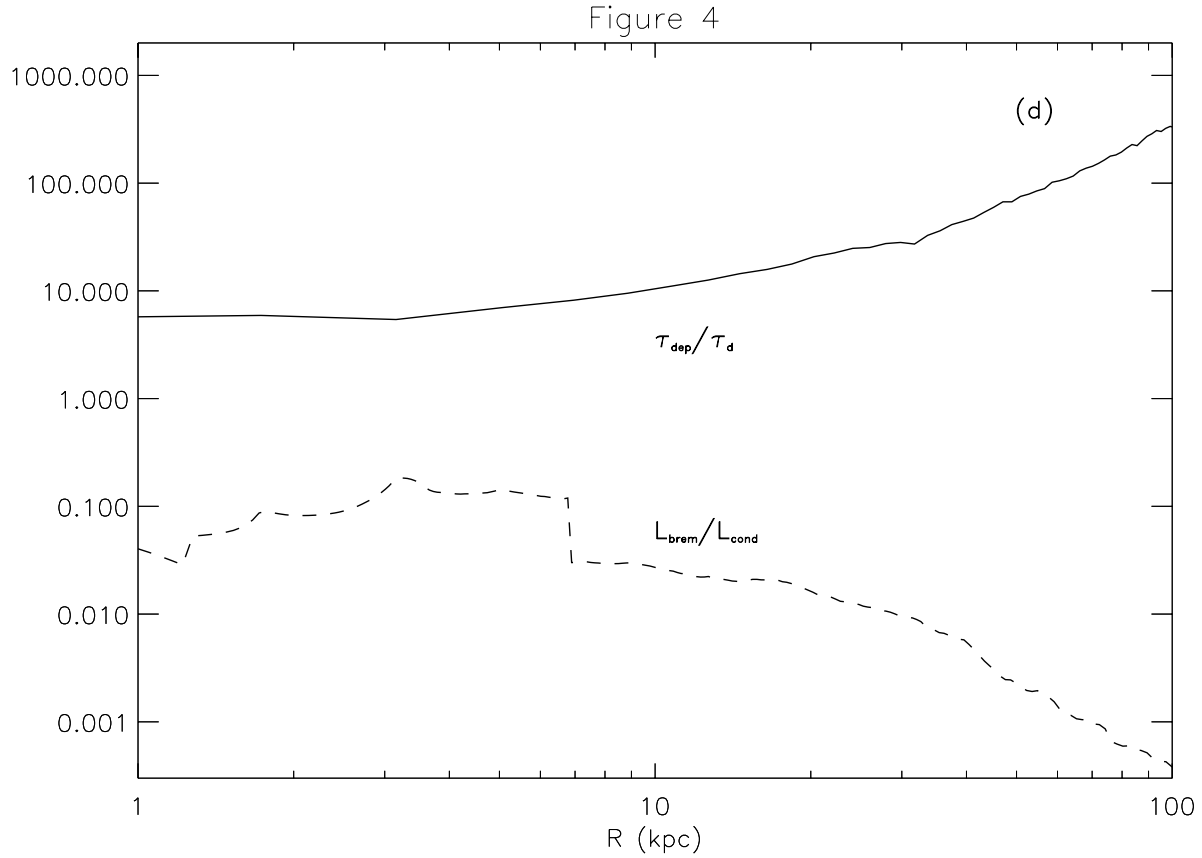


Fig. 4.— Model 3, with $f = 0.1$, at $10^9$ yr, displayed as in Figure 2. The effect of $f < 1$ is to reduce the heating of the RHG by motion of the WFC, and the comparison with Model 1 is similar to that of Model 2. Relative to Model 1, the mean density of the warm gas in Model 3 is comparable, whereas the density of the RHG is lower by an order of magnitude at small radii, and more at large radii. The filling factor of the warm clouds is therefore at least an order of magnitude larger in Model 3 than in Model 1, and reaches unity at large radii. The reduced pressure of the RHG relative to Model 1 leads to reduced densities in the WFC's and therefore a reduced star formation rate. The stellar density of Model 3 is therefore lower by an order of magnitude relative to Model 1. The lower density of the RHG also leads to conductive losses dominating bremsstrahlung emission in the hot phase at all radii.

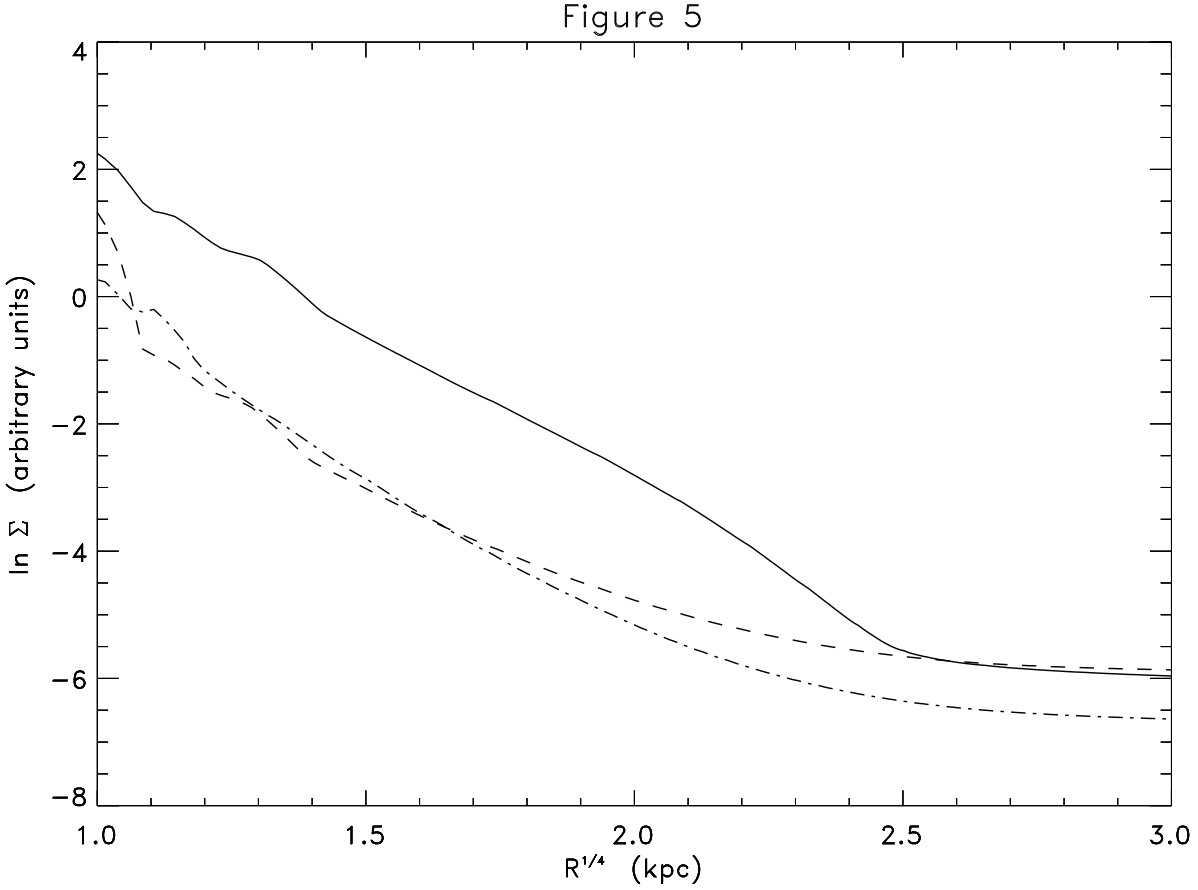


Fig. 5.— The project stellar surface densities of Model 1 (solid), Model 2 (dashed), and Model 3 (dot-dashed).

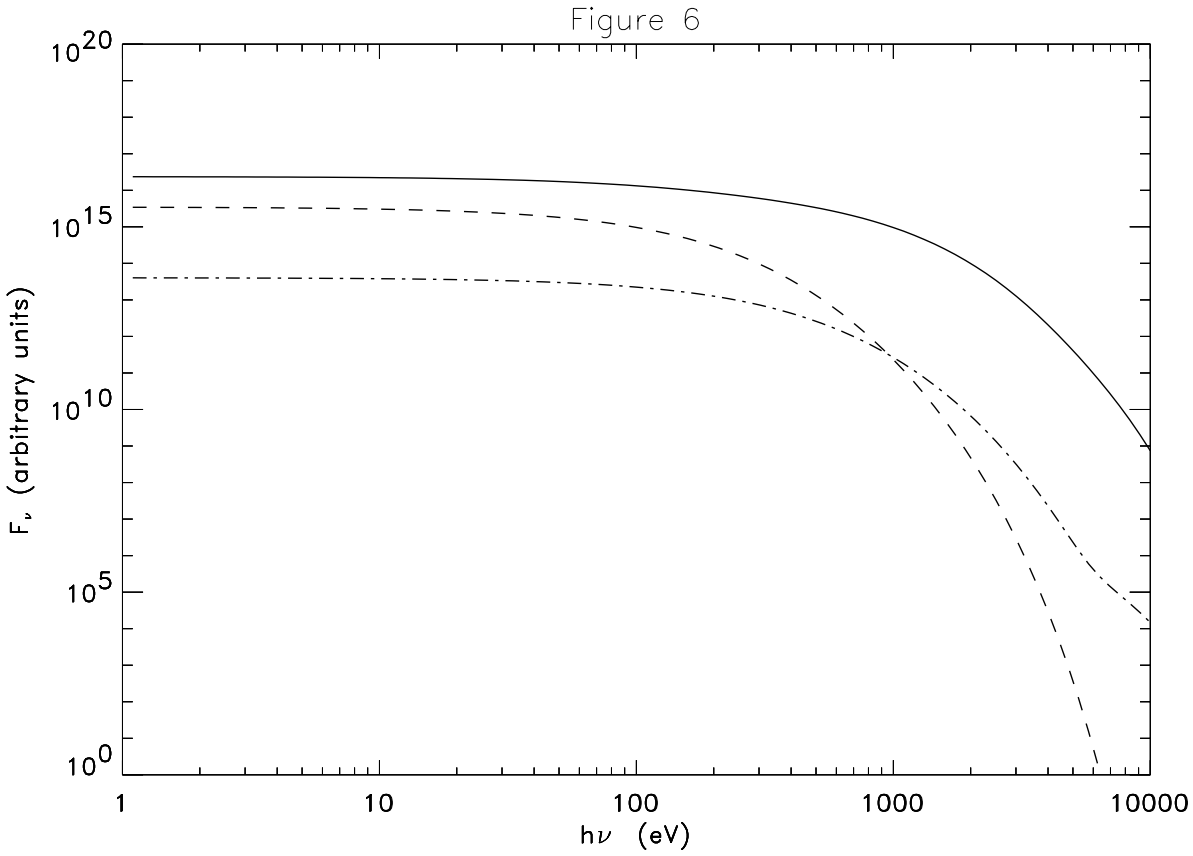


Fig. 6.— The spectral energy distributions (in arbitrary units) of Model 1 (solid), Model 2 (dashed) and Model 3 (dot-dashed), as determined by assuming bremsstrahlung emission at the temperature of the RHG.